Comparison of the kinetics and spectral properties of $AuCl_4^-$ binding by methanobactins from *Methylosinus trichosporium* Ob3b and *Methylocystis* strain sb2: Evidence of exciton disruption between intramolecular chromophores

by

Erick Alan Turpin

A thesis submitted to the graduate faculty

in partial fulfillment of the requirements for the degree of

MASTER OF SCIENCE

Major: Biochemistry

Program of Study Committee:
Alan A. DiSpirito, Major Professor
Amy Andreotti
Steven Rodermel

Iowa State University

Ames, Iowa

2016

DEDICATION

This work is dedicated to the memory of my father, David Alan Turpin

TABLE OF CONTENTS

"Reality is merely an illusion,

albeit a very persistent one."

- Albert Einstein

ACKNOWLEDGMENTS

I would like to extend my genuine thanks to my committee members: Dr. Steven Rodermel, who was the first among all of my professors to suggest to me that I pursue a graduate education, somewhat insistently; Dr. Amy Andreotti, who later encouraged me, not only by introducing me to one of my greatest scientific passions, but also by recommending me to pursue graduate studies; and especially my major professor Dr. Alan DiSpirito. I truly cannot thank you enough for the opportunity that you afforded me to prove myself and my abilities.

It is here that I would also care to thank those members, both faculty and staff, of the Roy J. Carver Department of Biochemistry, Biophysics, and Molecular Biology. A special and profound thanks to Desi Gunning, whose guidance and belief in me, has proved to be one of the most valuable assets in my educational tenure. Thanks to all the people with whom I have worked over the years, particularly Dr. Nathan Bandow and Bipin Baral, who took time to patiently train me and answer my questions.

Finally, I would like to extend my thanks to my friends and family. Particularly my mother, for her advice and unwavering support through the difficult times that I encountered along the way, both academic and personal. Without any doubt, I would not have made it this far without her.

ABSTRACT

Methanobactin (Mb) is the first characterized example of a chalkophore or copper binding protein. Mbs are produced by most aerobic methane oxidizing bacteria for Cu recruitment to the cell and eventually incorporation into the central metabolism. In addition to the biological purpose of Cu binding, mbs bind some transition and near transition metals. Within this text, the metal binding properties are explored and compared between two mbs, which represent two distinct groups of mbs, mb from *Methylosinus trichosporium* OB3b and mb from *Methylocystis* strain SB2. The Cu binding properties of these mbs have been previously explored, however, herein, the binding and displacement properties of each mb are presented for a number of transition metals.

The binding properties of the metals able to displace Cu^{+} from Cu^{+} bound mb (Cu-mb) are of particular interest, due to the extremely high affinity with which mbs bind Cu^{2+}. Mercury is one such example, and the binding properties of Hg, in the forms Hg^{2+}, $Hg(CN)_2$, and CH_3Hg^{+}, are examined for mb from *Methylocystis* strain SB2. Each form was bound slightly differently by mb-SB2. Chapter 2 presents the characterization of the Hg binding, in each form, for mb-SB2.

Gold also displaces Cu-mb for both mb-OB3b and SB2. In the final chapter, the $AuCl_4^{-}$ binding properties of mb-OB3b and mb-SB2 are compared. Previously collected CD spectra of mb-SB2 titrated with $AuCl_4^{-}$ suggested that an exciton transfer exists between the chromophores of mb-SB2. Herein, stopped flow UV-vis kinetic traces of mb-OB3b titrated with $AuCl_4^{-}$ demonstrate that an exciton transfer is present between the chromophores of mb-OB3b.

CHAPTER I:

GENERAL INTRODUCTION

Structure and function of methanobactins

Methanobactins are small polypeptides, less than 1200 Da, produced by many aerobic methane oxidizing bacteria. Methanobactins are responsible for the recruitment of copper from the local environment. A peptide that recruits copper for biological assimilation is called a chalkophore, named after the very similar function performed by siderophores, which recruits iron for biological assimilation. The term 'chalkophore', which literally means "copper bearing", comes from the Greek, "*chalkós"*, meaning "copper" and "*phoros*", meaning "bearing". Methanobactins are the first known example of a chalkophore, which binds copper and assimilates that copper into the metabolism [3].

Mbs have a general chemical structure consisting of two 5 or 6 member rings, one oxazolone ring and another oxazolone, imidazolone, or a 6 membered pyrazinedione ring, which are separated by 2-5 amino acids, each ring associated with a thioamide [3,7,11]. The rings of the mb together with their associated thioamides, form the binding site for copper and other metals [3,11]. The mbs from *Methylosinus trichosporium* OB3b and *Methylocystis* strain SB2 both fall within the α-Proteobacteria group, but are categorized into two groups based on their catabolic activity and structure. The first class of mbs (group 1), corresponding to those falling under the mb-OB3b category, are typically larger than the group 2 mbs, and can produce either the particulate methane mono-oxygenase (pMMO) and the soluble methane mono-oxygenase (sMMO). Mb-SB2,

which is a group 2 mb, does not contain the genes for the sMMO, and therefore can only express the pMMO gene product for methane oxidation.

The most important structural difference between mbs-OB3b and SB2 is the presence of the cysteine residues in the mature form of the peptide. Mb-OB3b has two cysteine residues that are linked in a disulfide bond that lends structure and stability to the peptide and the metal bound structure (Figs. 1A and 2A) [4,9,11]. In contrast, mb-SB2 has no cysteine residues, which are thought to be assimilated into the ring structures of mb-SB2 based on the location of those residues in the peptide, and therefore has no disulfide bond (Figs 1B and 2B). Mb-SB2 does, however, contain an additional sulfate group, not present in mb-OB3b, which aids in the sharp turn associated with the metal bound structure of mb-SB2 (Figure 2B).

Metal Binding, Reduction, and Displacement by Methanobactins

The binding of Cu^{2+} and Cu^{+} by mbs-OB3b and SB2 have been previously characterized spectrally, kinetically, and thermodynamically [2]. Mbs bind copper with very high affinity, having binding constants as high as $3.3 \times 10^{34} \pm 3.0 \times 10^{11}\ M^{-1}$ [2]. The proposed coordination of metals by the mbs-OB3b and SB2 in a 1 to 1 ratio is shown in figure 2.

In addition to Cu^{2+} and Cu^{+}, the binding characteristics for some transition metals have been explored for both mbs-OB3b and SB2. Specifically, the metals Fe^{3+}, Au^{3+}, Cd^{2+}, Co^{2+}, Zn^{2+}, Mn^{2+}, Ni^{2+}, Hg^{2+}, Pb^{2+}, Cu^{2+}, and Ag^{+} were tested and found to be bound by both mbs-OB3b and SB2 [8,9]. When bound by mb-OB3b, Cu(II) is reduced to Cu(I) [9]. Two of the transition metals bound by mb-OB3b are also reduced when

bound, these include: Au(III), which is reduced to Au(0), and Hg(II), which is reduced to Hg(0) [2,8]. The same is true of mb-SB2, which reduces Au(III) to Au(0), and forms nanoparticles in the process. Mb-OB3b has been recently shown to reduce up to 19 Au(III) to Au(0) without an external reductant, and, in the presence of an external reductant, will indefinitely reduce Cu(II) and Au(III) to Cu(I) and Au(0), respectively [8].

Despite a high affinity for copper, a few transition metals displace copper bound mb (Cu-mb), as determined by UV-visible spectrum, collected prior to and after addition of equimolar copper and the displacing metal to that of the mb solution, 50 μM, to a final mole ratio of 1:1:1 (mb: Cu^{2+}: M). Where M is a generic placeholder for the displacing metal in question. The binding of many transition and near transition metals has been reported previously, however only a few displace copper from Cu-mb. Interestingly, the metals that are successful in displacing copper from Cu-mb are not consistent between mb-OB3b and mb-SB2, which indicates that the two groups of mbs have distinct metal binding and metal displacement profiles.

A complete listing of the metals tested for displacement against Cu-mb, gold bound mb (Au-mb), and mercury bound mb (Hg-mb) are listed below for mb-SB2 and for mb-OB3b (Tables 1 and 2, respectively).

Exciton Transfer

In an exciton transfer a photon of light is passed back and forth between two chromophores, each chromophore exciting and being excited by the other. When those chromophores reside in the same molecule, circular dichroism (CD) spectra can be used to determine the relative position and orientation of the chromophores [13]. Cotton

effects or couplets appear in the CD spectra of those molecules engaging in exciton transfer. These couplets, which are directly related to the chirality of the electric dipoles between chromophores [12], indicate the relative orientation of the two chromophores with respect to each other [12,13].

Exciton transfers have been shown to occur between the two rings in mb [7], which is demonstrated through spectral data, such as CD and fluorescence spectra. The Cotton effects present in the CD spectra when titrated with $AuCl_4^-$ [10], as well as the increased emission intensity following addition of $AuCl_4^-$ in the fluorescence spectra are consistent with intramolecular exciton transfer between the chromophores of mbs-OB3b and SB2 [3]. Herein, kinetic data indicating the disruption of an exciton transfer, between the oxazolone rings during the binding of $AuCl_4^-$, is presented, along with the related spectral evidence, as further visible evidence of exciton transfer between the rings of mb.

Thesis Organization

The second chapter covers the binding of mercury, in the forms: Hg^{2+}, $Hg(CN)_2$ and CH_3Hg^+, by mb-SB2 is examined. Mercury binding occurs differently based on the form of the mercury molecule. Spectral evidence suggests Hg^{2+} binds to both the oxazolone and imidazolone rings, whereas, CH_3Hg^+ appears to only bind to the oxazolone ring. Spectrally, $Hg(CN)_2$ falls somewhere between Hg^{2+} and CH_3Hg^+. Additionally, the thermodynamic data suggest that the binding of each Hg ligand is complex, involving a 3 or 4 site model.

Within the contents of chapter 3, the kinetics and spectral properties of $AuCl_4^-$ binding are compared between the mbs-OB3b and SB2. The evidence presented therein demonstrates the presence of an intramolecular exciton transfer between the chromophores of each mb. The exciton transfer is not observable in the kinetics of $AuCl_4^-$ binding by mb-SB2, because the reaction completes within the 1.4 ms mixing time of the instrument used to collect the kinetics data. Fortunately, the binding of $AuCl_4^-$ by mb-OB3b, at chilled temperatures, was slow enough so that the exciton transfer disruption was captured in the kinetic traces. Those traces are presented in this section, along with the supporting spectral evidence for intramolecular exciton transfer for both mbs-OB3b and SB2.

Based on the results obtained, the evidence supports the model proposed previously, with respect to mole ratio [1,2]. However, the results do show that in contrast with the binding model, therein proposed, that the binding of $AuCl_4^-$ occurs in the reverse order with respect to the rings involved in the binding of the ligand. The circular dichroism (CD) spectra and fluorescence spectra collected for the titrations of mb-SB2 and mb-OB3b with $AuCl_4^-$, also suggest an exciton transfer between the chromophores. However, prior to collection of the UV-vis stopped flow traces for the titration of mb-OB3b by $AuCl_4^-$, the presence of an exciton had not been previously detected because the reaction was complete or nearly complete in the 1.4 ms mixing time of the instrument. Those traces revealed direct evidence of a disruption in exciton transfer between the oxazolone chromophores of mb-OB3b.

Figures

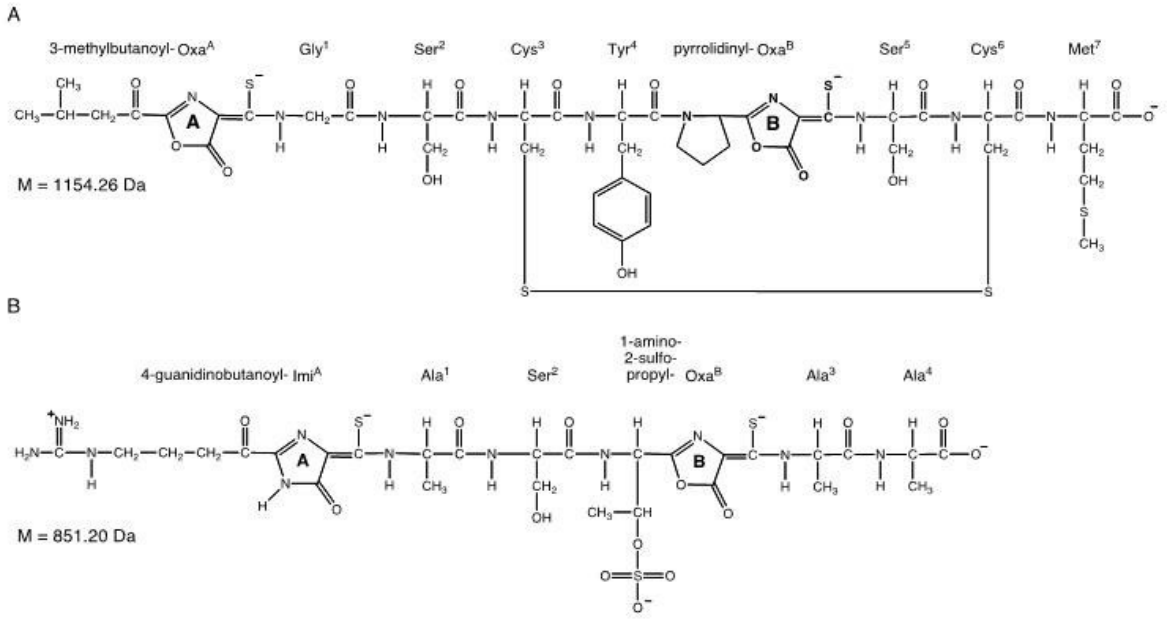

Figure 1. Chemical structure and the associated molecular weights of methanobactin from *Methylosinus trichosporium* OB3b (A) and *Methylocystis* strain SB2 (B).[3]

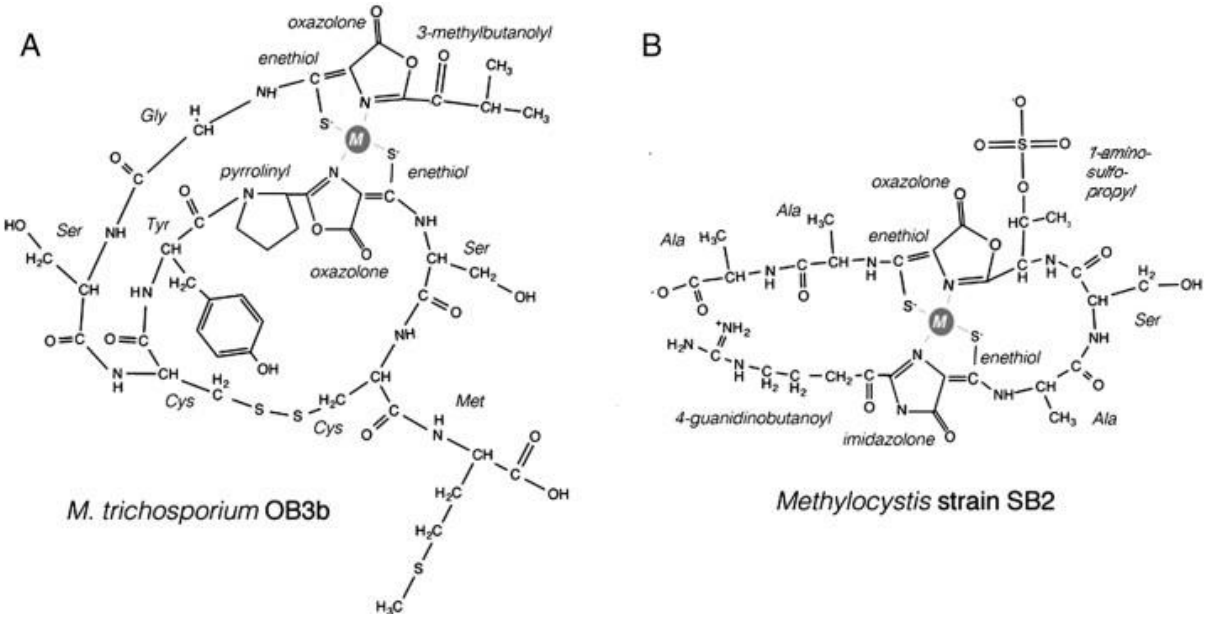

Figure 2. Proposed metal coordination structure by mb-OB3b (A) and mb-SB2 (B).

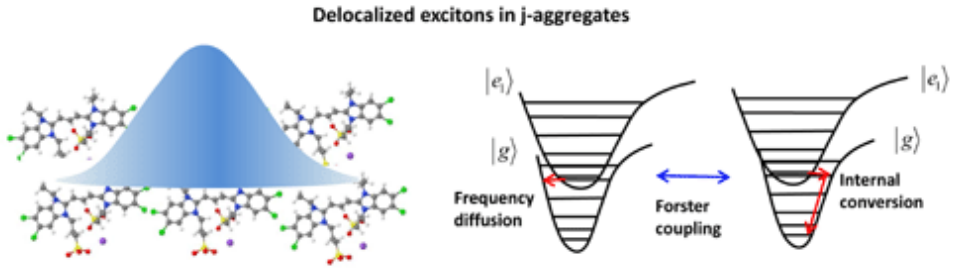

Figure 3. Forster coupling of J-states leading to exciton transfer between chromophores.

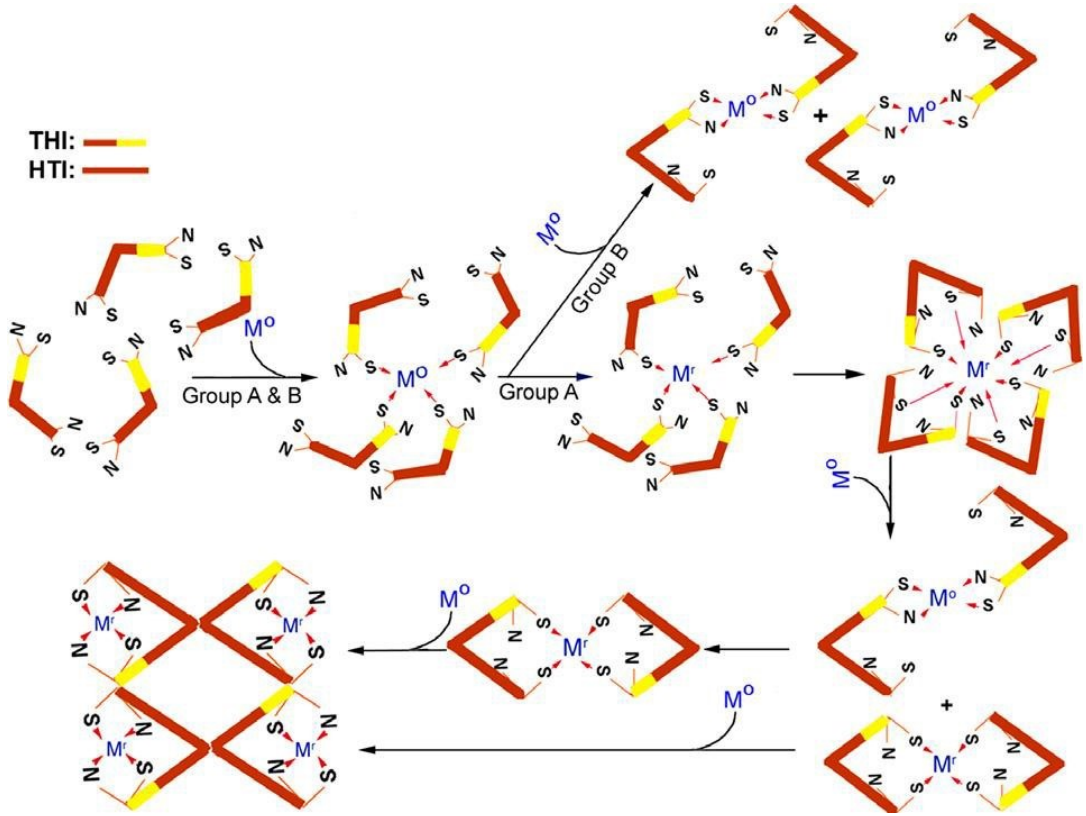

Figure 4. Metal binding model previously proposed for metal binding of group A metals (Ag(I), Au(III), Cu(II), Hg(II), Pb(II), and U(VI) as well as group B (Cd(II), Co(II), Fe(III), Ni(II), and Zn(II), which is characterized by a decrease in the number of methanobactins coordinating the metal ligand with increasing metal to methanobactin ratio. Starting with an oligomer or tetramer coordination, moving to a dimer coordination, and finally each metal ligand is bound by a single methanobactin. Note: HTI – oxazolone A; THI – oxazolone B

Tables

Table 1. Mb-SB2 Metal Binding/Displacement Table.
"+": indicates that the competing metal was bound preferentially to the initial metal bound in reaction mixtures of 1:1:1 at 50μM ([mb-SB2]:[$M_{Initial}$]:[$M_{Competing}$]); "-": indicates that the competing metal was not bound preferentially to the initial metal bound in reaction mixtures of 1:1:1 at 50μM ([mb-SB2]:[$M_{Initial}$]:[$M_{Competing}$]).

mb-SB2		Initial Metal Bound									
		$FeCl_3$	$CoCl_2$	$ZnSO_4$	$CdCl_2$	$MnSO_4$	$NiCl_2$	$HgCl_2$	$Pb(NO_3)_2$	$CuSO_4$	$AgNO_3$
Competing Metals	$CuSO_4$	+	+	+	+	+	+	+	+	x	+
	$HAuCl_4$	+	+	+	+	+	+	-	+	+	+
	$HgCl_2$	+	+	+	+	+	+	x	+	+	+
	$Pb(NO_3)_2$	+	+	+	-	+	+	-	x	+	+

Table 2. Mb-OB3b Metal Binding/Displacement Table.
"+": indicates that the competing metal was bound preferentially to the initial metal bound in reaction mixtures of 1:1:1 at 50 µM ([mb-OB3b]:[$M_{Initial}$]:[$M_{Competing}$]); "-": indicates that the competing metal was not bound preferentially to the initial metal bound in reaction mixtures of 1:1:1 at 50µM ([mb-OB3b]:[$M_{Initial}$]:[$M_{Competing}$]).

mb-OB3b		Initial Metal Bound									
		$FeCl_3$	$CoCl_2$	$ZnSO_4$	$CdCl_2$	$MnSO_4$	$NiCl_2$	$HgCl_2$	$Pb(NO_3)_2$	$CuSO_4$	$AgNO_3$
Competing Metals	$CuSO_4$	+	+	+	+	+	+	-	+	x	-
	$HAuCl_4$	+	+	+	+	+	+	+	+	+	+
	$HgCl_2$	+	+	+	+	+	+	x	+	+	+
	$Pb(NO_3)_2$	+	+	+	-	+	-	-	x	-	-

References

[1] Choi, D. W.; Do, Y. S.; Zea, C. J.; McEllistrem, M. T.; Lee, S.-W.; Semrau, J. D.; Pohl, N. L.; Kisting, C. J.; Scardino, L. L.; Hartsel, S. C.; Boyd, E. S.; Geesey, G. G.; Riedel, T. P.; Shafe, P. H.; Kranski, K. A.; Tritsch, J. R.; Antholine, W. E.; DiSpirito, A. A.; *J. Inorg. Biochem.* 2006, 100: 2150–2161.

[2] Choi, D. W.; Zea, C. J.; Do, Y. S.; Semrau, J. D.; Antholine, W. E.; Hargrove, M. S.;Pohl, N. L.; Boyd, E. S.; Geesey, G. G.; Hartsel, S. C.; Shafe, P. H.; McEllistrem, M. T.; Kisting, C. J.; Campbell, D.; Rao, V.; la Mora, de, A. M.; DiSpirito, A. A.; *Biochemistry* 2006, 45: 1442–1453.

[3] Bandow, N.; Gilles, V. S.; Freesmeier, B.; Semrau, J. D.; Krentz, B.; Gallagher, W.; McEllistrem, M. T.; Hartsel, S. C.; Choi, D. W.; Hargrove, M. S.; Heard, T. M.; Chesner, L. N.; Braunreiter, K. M.; Cao, B. V.; Gavitt, M. M.; Hoopes, J. Z.; Johnson, J. M.; Polster, E. M.; Schoenick, B. D.; Umlauf, A. M.; DiSpirito, A. A.; *J. Inorg. Biochem.* 2012, 110: 72–82.

[4] Ghazouani, El, A.; Baslé, A.; Firbank, S. J.; Knapp, C. W.; Gray, J.; Graham, D. W.; Dennison, C.; *Inorg. Chem.* 2011, 50: 1378–1391.

[5] Berova N, Di Bari L, Pescitelli G.; *Chem Soc Rev.* 2007 Jun;36(6):914-31.

[6] Lightner, D. A.; Gurst, J. E; Wiley-VCH: New York, NY, USA, 2000.

[7] DiSpirito AA, Semrau JD, Murrell JC, Gallagher WH, Dennison C, Vuilleumier S. *Microbiol Mol Biol Rev*. 2016 Mar 16;80(2):387-409.

[8] Bandow, Nathan, "Isolation and binding properties of methanobactin from the facultative methanotroph Methylocystis strain SB2" (2014). Graduate Theses and Dissertations. Paper 13910.

[9] H.J. Kim, D.W. Graham, A.A. Dispirito, M.A. Alterman, N. Galeva, C.K. Larive, et al., *Science.* 305 (2004) 1612–1615.

[10] E.A. Turpin, B.S. Baral, N.L. Bandow, J.D. Semrau, A.A. DiSpirito, unpublished.

[11] El Ghazouani A, Basle A, Gray J, Graham DW, Firbank SJ, Dennison C. 2012. *Proc Natl Acad Sci U S A* 109: 8400-8404

[12] Person RV, Monde K, Humpf HU, Berova N, Nakanishi K. *Chirality*. 1995;7(3):128-35.

[13] Berova N, Di Bari L, Pescitelli G.; *Chem Soc Rev*. 2007 Jun;36(6):914-31.

CHAPTER II

MERCURY BINDING BY METHANOBACTIN FROM *METHYLOCYSTIS* STRAIN SB2

Bipin S. Baral, Nathan L. Bandow, Alexy Vorobev, Brittani C. Freemeier, Brandt H. Bergman, Timothy J. Herdendorf, Nathalie Fuentes, Luke Ellias, Erick Turpin, Jeremy D. Semrau and Alan A. DiSpirito

Abstract

Methanobactin (mb) is a post-translationally modified copper-binding compound or chalkophore secreted by many aerobic methane oxidizing bacteria (AMOB) in response to copper limitation. In addition to copper, methanobactin from *Methylosinus trichosporium* OB3b (mb-OB3b) has been shown to bind a variety of metals including Hg^{2+}. In this report, Hg binding by the structurally unique methanobactin from *Methylocystis* strain SB2 (mb-SB2) was examined and compared to mb-OB3b. Mb-SB2 is shown to bind the common forms of Hg found in the aqueous environments, Hg^{2+}, $Hg(CN)_2$ and CH_3Hg^+. The spectral and thermodynamic properties of binding for each form of mercury differed. UV-visible absorption spectra suggest Hg^{2+} binds to both the oxazolone and imidazolone rings, whereas, CH_3Hg^+ appears to only bind to the oxazolone ring. $Hg(CN)_2$ shows spectral properties between Hg^{2+} and CH_3Hg^+. Isothermal titration calorimetry (ITC) showed both $Hg(CN)_2$ and CH_3 Hg^+ fit into two site binding models. For $Hg(CN)_2$ the first site was exothermic and the second endothermic. Both binding sites in CH_3Hg^+ were exothermic, but at equilibrium never

moved back to zero. ITC results for Hg^{2+} was more complex and suggested a 3 or 4 site model.

The spectral, kinetic and thermodynamic changes following Hg binding by mb-SB2 also differed from the changes associated with mb-OB3b. Like mb-OB3b, copper did not displace Hg bound to mb-SB2. However, in contrast to mb-OB3b, Hg^{2+} could displace Cu from Cu- containing mb-SB2 and preferentially bound Hg^{2+} over Cu^{2+} at metal to mb-SB2 molar ratios above 1.0.

Introduction

Methanobactin (mb) is a small, <1,200 Da, post-translationally modified, copper binding compound or chalkophore produced by many aerobic methane oxidizing bacteria (AMOB) and potentially several non-AMOB bacteria as well based on bioinformatic analyses [1 – 4]. The molecule has been structurally characterized in 5 different AMOB [3, 5 – 8] and this class of metal binding peptides are characterized by the presence of one oxazolone ring and a second five or six membered ring, which is either an oxazolone, imidazolone or a pyrazinedione ring (Fig. 1) [3]. Both rings are associated with an enethiol group, which together or forms the metal coordination site. Depending on the metal, the coordination site consists of one of the rings and its associated enethiol or both rings and associated enethiols [Table S1; 9]. The two rings are separated by 2 to 5 amino acids. Although structurally unique, the copper binding properties of mb-OB3b and mb-SB2 were similar, suggesting the pair of rings and associated enethiols confer the unique metal binding properties associated with this class of metal binding peptides [1, 6, 7, 10 – 14].

In addition to copper, mb from *M. trichosporium* OB3b (mb-OB3b) has also been shown to bind all tested transition and near transition metals (Table S1) [9, 19]. In general, the binding constants for most of the metals are well below those observed for copper and copper will displace most other metals bound to mb-OB3b [9]. However, some metals, such as Au^{3+}, Hg^{2+}, and Pb^{3+} appear to have binding properties similar to Cu^{2+}, and Cu^{2+} cannot displace these metals [9]. A recent study by Vorobev *et al*. [19] demonstrated that mb-OB3b reduced Hg toxicity to *M. trichosporium* OB3b as well as to other methanotrophs even in the presence of Cu^{2+}. The study also showed that when exposed to equimolar concentrations of Hg (II) and Cu(II), mb-OB3b will bind approximately 1 Hg for every 10 Cu. Here we extend current analyses of Hg binding by chalkophores by examining the mechanism of Hg binding in the structurally unique mb from *Methylocystis* species SB2 (Fig. 1) (mb-SB2). With the exception of the core methanobactin features stated above, the structure of methanobactin from *Methylocystis* strain SB2 differs dramatically from mb-OB3b (Fig. 1). In mb-SB2 the redox active and metal binding amino acids found in mb-SB2 are replaced with Ala or are missing. The disulfide bond providing structural stability in mb-OB3b is also missing in mb-SB2. Thus, a comparison of the properties between the two methanobactins provides means to assist the role of the protein backbone in the metal binding properties of the methanobactin.

Materials and Methods

Growth and isolation of mb-SB2

Methylocystis strain SB2 was cultured for mb-SB2 production in NMS medium [20] in sequential batch reactors. To maintain high (20 – 50 μM) concentrations of mb-SB2 in the spent media the copper concentrations in the reactor were varied, with two turnovers of NMS media containing 0.2 μM Cu followed by a one turnover of NMS media containing 1.0 μM CuSO4. This sequence was generally repeated 2 to 4 times. Varying copper concentrations in the culture media maintained high culture density and high concentrations of mb-SB2 in the spent media.

Mb-SB2 was isolated from the spent media as previously described [16]. Purity of mb- SB2 samples was determined as previously described [3,8,10,11,16]. Sample purity was > 97%, with breakdown fragments of mb-SB2 comprising most of trace contaminates. Mb-SB2 samples used in this study contained less than 0.02 Cu per mb-SB2 as determined by atomic absorption spectroscopy described below. Following purification, the samples were stored in the dark.

Acid hydrolysis of mb-SB2

Acid hydrolysis of the oxazolone ring in mb-SB2 was carried out in reaction mixtures containing 50μM mb-SB2 in 85μM acetic acid. The reaction mixtures were incubated at 25^{o} C for 7-9 h and the monitored by UV-visible spectroscopy to determine the time required for the complete hydrolysis of the oxazolone ring. In contrast to the procedure reported by Krentz et al. [3], the final pH of the solution was 6.8 and therefore

did not require neutralization. The hydrolyzed solutions were kept on ice and used within 12 h of preparation.

Spectroscopy

UV-visible absorption, fluorescent, and circular dichroism spectroscopy were performed as previously described [10, 16]. Briefly, either 50μM (for UV-visible absorption and fluorescence) or 500 μM (for UV-visible CD) mb-SB2 solutions were prepared in > 18MΩ▪cm H2O and titrated with 10 mM metal stock solutions of metals also prepared in > 18MΩ▪cm H2O. Titrations involved sequential 0.05 or 0.1 molar additions of metal to mb-SB2 pre-loaded into a cuvette and rapidly mixed by hand for 10 – 20 sec. Spectra were taken immediately after mixing.

Protein and metal determination

Protein was determined by the Lowry method [21]. Copper and mercury were determined on an Agilent 55AA atomic absorption spectrometer (Agilent Technologies Inc., Santa Clara, CA) coupled with a vapor diffusion VGA 77 system and run in either the flame or cold vapor mode for copper and mercury, respectively. All measurements were taken in triplicate. Mercury volatilization was determined as described by Takeuchi *et al.* [22] and modified as previously described by Vorobev, *et al.* [19].

mb-SB2 mediated solubility of Hg^0

The solubility of Hg^0/Hg^{2+} in the aqueous phase was determined by incubating Hg^0 in > 18MΩ▪cm H2O at room temperature. Reaction solutions contained 25 μl Hg^0 in

25 ml of > 18MΩ▪cm H2O with and without the addition of 50µM mb-SB2 or 50µM bovine serum albumin (BSA). Reaction mixtures were incubated at room temperature with continuous stirring. Periodically, the stirring was stopped for 30 sec and 1ml of the solution was removed from the top and diluted with 14 ml of 5% HCl, 5 % HNO3 and 90% H2O (v/v). Hg in the aqueous phase was determined by metal analysis as described above. Similar experiments were performed under anaerobic conditions in an atmosphere of 96% argon and 4% hydrogen inside an anaerobic chamber (Coy Laboratories, Michigan, United States). The presence of O2 inside the chamber was monitored via a Coy oxygen/hydrogen meter and by anaerobic indicator strips (Oxoid Ltd, Hants, UK). All solutions were also checked for oxygen contamination before and after each experiment using Oxoid anaerobic indicator strips. Mercury concentrations in the aqueous phase were determined by atomic absorption spectroscopy in vapor diffusion mode as described above. Reaction mixtures containing mb-SB2 were also examined by UV-visible absorption spectroscopy. For spectral analysis of samples incubated under anaerobic conditions, the reaction mixtures were loaded into septa-sealable cuvettes, sealed in the Coy chamber and the spectra taken outside the chamber.

Kinetics of mercury and copper binding to mb-SB2

The rates for mercury and copper binding to mb-SB2 were determined by measuring absorption changes at 341nm and 389 nm, using a four-syringe Biologic SFM/4000/S stopped flow reactor coupled to a MOS-500 spectrophotometer (Bio-Logic Science Instrument SA, Claix, France). Metal stock solutions of $CuCl_2$, $HgCl_2$, or $Hg(CN)_2$ were prepared in > 18MΩ▪cm H2O. The stock solutions for mb-SB2 were

prepared by dissolving freeze-dried mb- SB2 mb in > 18MΩ▪cm H2O. The stock solutions of $CuCl_2$, $HgCl_2$ and mb-SB2 were chilled on ice then filtered through 0.22 µm filter before loading into sample syringes. The final concentration of the stock mb-SB2 after filtration was determined by UV-visible absorption spectroscopy as previously described [15]. The path length for the cuvette used in the Biologic SFM/4000/S stopped flow reactor was 1.5 mm. The dead time of the system was 1.4 ms. The system was cooled and maintained at 4° C. The reaction mixture contained 400 µM of mb-SB2 and either 40, 100, 200, 240, 280, 320, 360, 400, 600, 700, or 800 µM of $CuCl_2$, $HgCl_2$, or $Hg(CN)_2$. Rates obtained for each concentration was an average of a minimum of 5 traces. Traces following metal addition were divided by traces from 0 metal additions before the traces were fit. The rates were determined by fitting the traces to the exponential function in Biokine operational software (Bio-Logic Science Instrument SA). Binding rates were calculated in mol metal bound per sec per mol mb-SB2 and reported as the binding rate (sec-1).

Copper and mercury mixed-metal binding experiments

Binding of mercury and copper in mixed metal conditions by mb-SB2 were determined in solutions containing $CuCl_2$, $HgCl_2$, $Hg(CN)_2$ or CH_3HgCl and mb-SB2 in molar ratios of metal to methanobactin of 0.25:0.25:1, 0.5:0.5:1, 1:1:1, 1.5:1.5:1, and 2:2:1. The solutions were incubated with stirring (200 rpm) at room temperature for 5 min. Following the incubation period the samples were loaded to pre-equilibrated Sep-Pak cartridges (Millipore Corporation, Billerica, MA USA) as previously described [15]. Sep-Pak cartridges contain hydrophobic reverse-phase C-18 resin, to separate

methanobactin from unbound metal. Sep-Pak cartridges were washed with 6 ml of > 18MΩ▪cm H2O three times then eluted with 6 ml of 60 % acetonitrile: 40% H2O. Copper and mercury measurements were determined as described above in the reaction mixture, in the wash solution as well as in the sample eluent. Similarly, copper and mercury measurements were performed on control solutions containing: i) mercury and copper only, ii) mercury and mb-SB2 only and iii) copper and mb-SB2 only.

Displacement of mb-SB2-bound metals

Displacement of a metal bound to mb-SB2 was determined by the changes in UV-visible absorption spectra following the addition of $HgCl_2$, $Hg(CN)_2$ or CH_3HgCl to and in selected samples by metal analysis. AgCl, $FeCl_3$, $CdCl_2$, $CoCl_2$, $NiCl_2$, $ZnSO_4$, $PbNO_2$, or $CuCl_2$ was added to mb-SB2 in a molar ratio of 1.1 metal per mb-SB2 and the UV-visible absorption spectrum between 200 and 500 nm determined. A second metal, either $HgCl_2$, $Hg(CN)_2$ or CH_3HgCl was then added in equimolar concentrations and the UV-visible absorption spectra determined. The UV-visible absorption spectra for each metal bound to mb-SB2 is unique (results not shown) and was used to determine displacement. The potential displacement of Cu(II) by $HgCl_2$, $Hg(CN)_2$ or CH_3HgCl were also assayed by metal analysis as described above for mixed-metal binding experiments.

Isothermal titration calorimetry (ITC)

ITC was performed at 25°C using a GE Microcal ITC200 microcalorimeter (GE Health Sciences, Piscataway, NJ, USA). Titrant solutions were 0.35, 1.0 or 4 mM CH_3HgCl, $HgCl_2$ and $Hg(CN)_2$. $HgCl_2$ and $Hg(CN)_2$ were prepared in > 18MΩ▪cm H2O.

100 mM CH_3HgCl stock solutions were prepared in CH_3OH and then diluted to 4 mM with H_2O with a final methanol concentration of 4% (v/v). The injections were added at 180 sec intervals, and based on the volume of injection the software predetermined the length of each injection. Injection volumes varied from 1-2 µl into a cell containing 100µM mb-SB2 with a stirring rate of 1000 rpm. The instrument was cleaned between experiments with > 18MΩ▪cm H2O, and the sample cell also washed according to manufacturer recommendations when sample build-up was observed. Following each titration, the sample cell was also washed with 1 – 3 cell volumes of 100 µM mb-SB2 to remove any residual metal. The data were analyzed using nonlinear least-squares curve fitting in Origin 7.0 software (GE Health Sciences). Due to fitting limitations of the software, some of the data was fit by hand and the other more unusual data curves had sections that could not be fit and were listed as unable to fit (UTF). Origin 7.0 software requires the data to return to zero in order to be fitted and in the case of CH_3HgCl binding to mb-SB2, the entire data curve was shifted along the y-axis by 2000 calories per mole to allow the curve to be fit by the software. Following this shift, the changes in enthalpy (ΔH) values were corrected by the magnitude of the shift before calculating the change in Gibbs free energy (ΔG). The stoichiometry for the binding of each form of mercury is indicated in Table 1 as calculated by the binding algorithm used by the Origin software as the N value.

Results

UV-visible absorption spectroscopy

The addition of $HgCl_2$, $Hg(CN)_2$, or CH_3HgCl to mb-SB2 showed absorption changes in the 240 to 300 nm range characteristic of metal-ligand charge transfer transitions in compounds containing thiol groups (Fig. 2) [23 – 27]. The shape, and absorption maxima in this spectral range has also been shown to differ for different metals bound to the same protein [23, 24], which is also observed in the spectra in this region for the three different forms of mercury (Fig. 2). Based on the UV-visible absorption spectra changes following $HgCl_2$ addition (Fig. 2A, B), Hg^{2+} appeared to bind to both the oxazolone (338 nm) and imidazolone (387 nm) rings of mb- SB2 as evidenced by a decreased absorbance at 338 and 387 nm associated with the oxazolone and imidazolone rings, respectively, between 0.1 and 0.7 Hg^{2+} per mb-SB2. This was accompanied by a red shift of the 387 nm maxima to 402 nm with an additional increased absorbance at higher Hg^{2+} to mb-SB2 molar ratios. CH_3Hg^+, however, appeared to only bind to the oxazolone ring as little or no absorbance change at 389 nm was observed (Figs. 2E and F). The UV-visible absorption spectral change following $Hg(CN)_2$ additions had properties in between $HgCl_2$ and CH_3HgCl and was saturated at 0.5 $Hg(CN)_2$ (Fig. 2C and D). It should be noted here that $Hg(CN)_2$ is soluble in H2O, but the dissociation constant is low and can form complexes such as Hg(CN)42- [28, 29]. The UV-visible absorption spectra as well as the kinetic, metal displacement, fluorescent spectra and thermodynamic data, described below, all suggest mb-SB2 binds $Hg(CN)_2$ or one of the Hg-CN complexes and not the dissociated Hg^{2+}.

Previous studies on mb from *Methylosinus trichosporium* OB3b (mb-OB3b) demonstrated that CH_3Hg^+ bound to both oxazolone A and oxazolone B [19]. In mb-OB3b, the two oxazolone rings are separated by five amino acids, while in mb-SB2 the two rings are separated by only two amino acids suggesting the imidazolone ring does not coordinate CH_3Hg^+ due to steric inhibition of the bulky methyl group. To test this hypothesis, the oxazolone group of mb-SB2 was selectively hydrolyzed, which may eliminate this apparent steric inhibition (Fig. S1). Based on the UV-visible absorption spectra of the acid hydrolyzed sample, the imidazolone group of acid-hydrolyzed samples of mb-SB2 failed to bind CH_3Hg^+ suggesting the imidazolone group does not bind this organic form of Hg (Fig. S1). Fluorescent spectra (Fig S2), however, demonstrated the acid-hydrolyzed sample does bind approximately one CH_3Hg^+ per mb-SB2.

The decreased absorption in the 240 – 300 nm range of suggests CH_3Hg^+ binds to the enethiol groups in the absence of the oxazolone ring (Fig 1S). Steric inhibition by methyl group may still be responsible for the inability of the imidazolone ring to coordinate CH_3Hg^+, but this inhibition could not be verified by elimination of the oxazolone ring.

Under aerobic conditions, mb-SB2 appeared to increase the solubility metallic Hg^0 as determined by the Hg in the aqueous phase and by the changes in the UV-visible absorption spectra of mb-SB2 in the reactions mixtures containing (Fig. S3). However, the UV-visible absorption spectral changes following incubation in the presence of Hg^0 were identical to Hg^{2+} suggesting Hg^0 was first oxidized to Hg^{2+} and then bound by mb-SB2 (Fig. 1 and S3). A similar result could be obtained by the addition of a non-reactive protein, bovine serum albumin again suggesting the adventitious binding of Hg^{2+} to mb-

SB2 following the chemical oxidation of Hg^0. To verify this observation, these experiments were repeated under anoxic condition. Under such conditions, no Hg was detected in the aqueous phase, nor were spectral changes observed in the mb-SB2 incubated in the reaction mixtures confirming mb-SB2 bound Hg^{2+} following the chemical oxidation of Hg^0 (results not shown).

Reaction mixtures to monitor for the presence of volatile Hg^0 were negative suggesting no reduction of Hg^{2+} to Hg^0. Reduction of Hg^{2+} was expected, since both mb-OB3b and mb-SB2 have been shown to reduce Cu^{2+} to Cu^+ and mb-OB3b to reduce Au^{3+} to Au^0 [9 – 11]. If reduction does occur, Hg remained associated with mb-SB2.

Fluorescence spectroscopy

With one exception, the fluorescent spectra following excitation at 341 nm and mercury additions to mb-SB2 differed from the spectra following copper addition [11]. As observed following copper additions, all three forms of mercury resulted in an increased emission at 427 – 440 nm (Fig. 3). In the case of Cu^{2+}, the increase in emission stopped at a copper to mb-SB2 molar ratios of 0.4 Cu per mb-SB2 [11]. With mercury, the increase in emission continued at Hg to mb-SB2 molar ratios between 2.0 and 6.0 depending on excitation wavelength and form of mercury added. In all cases, the increased emissions continued well beyond the saturation points for UV-visible absorption spectra), UV-visible CD spectra or ITC titrations (described below).

The increased emissions cannot be explained solely by internal quenching between the imidazolone and oxazolone rings, since a similar trend is observed following hydrolysis of the oxazolone ring (Fig. S2). In fact, as observed following Cu^{2+} additions

[11], the intensity of the emission spectra following Hg additions increased approximately two-fold following acid hydrolysis of the oxazolone ring (compare Fig. S2 and Fig. 3). As previously observed [11] the emission spectra at 417 nm following excitation at 341 nm and following hydrolysis of the ring suggest the fluorescent properties of mb-SB2 is associated with the imidazolone ring (Fig. S2). The increased emission may be due to the binding of Hg to other functional groups in the molecule or to Hg^{2+} reduction to Hg^{+} or Hg^{0} followed by aggregate formation [30], but could not be determined from the results in this study.

Following excitation at 394 nm and the addition of $HgCl_2$, $Hg(CN)_2$ or CH_3HgCl the emission at 610 nm decreased and the emission at 440 nm increased. The emission spectra at 440 nm following $HgCl_2$ addition was particularly unusual (Fig 3B). The emission at 440 nm increased in a broad peak between 0 and 1.0 Hg per mb-SB2, followed by a decrease between 1.0 – 2.0 Hg per mb-SB2, followed by a splitting of the peak at higher Hg to mb-SB2 molar ratios. As observed following excitation at 341 nm, the intensity of the emission spectra following Hg additions increased approximately two fold following acid hydrolysis of the oxazolone ring (Fig. S2).

UV-visible circular dichroism spectroscopy

As observed in mb-OB3b and other small molecules the UV-CD of mb-SB2 in the absence of added metal was of an unordered polypeptide with strong negative shoulders at 202 nm and 233 nm and a positive band at 294 nm (Fig. 4A). The addition of Cu^{2+} resulted in a shift of the 202 to 215 nm and increased positive intensity at 264 nm between 0.1 and 0.5 Cu per mb-SB2 followed by a decreased at higher Cu to mb-SB2

molar ratios (Fig. 4 B and E). The UV-CD spectra following addition of Hg^{2+} differed dramatically from the spectra following Cu^{2+} addition, with little to no changes in the 202 nm range and a major increased in absorption at 243 nm at Hg to mb-SB2 between 0.1 and 0.75 Hg per mb-SB2 followed by a decrease at higher Hg to mb-SB2 molar ratios (Fig. 4B and 4E verses Fig. 4C and 4F). The CD bands at 264 nm following Cu^{2+} addition or at 243 nm following Hg^{2+} can be assigned to the metal-enethiol charge transfer transitions that are observed at sub-saturating concentrations [24 – 26].

In contrast to the UV-CD spectra, the visible-CD spectra were complex following metal addition. The major properties of the CD spectra from mb-SB2 did not coincide with the absorption maxima suggesting potential charge transfer evens between the oxazolone and imidazolone rings (Fig. 4A) [31, 32]. Surprisingly, the intensity of the visible CD bands from mb-SB2 were approximately 100-fold high than observed with mb-OB3b, which is probably a reflection of the shorter distance between the oxazolone and imidazolone rings or to the absence of the disulfide bond in mb-OB3b. To assign the CD signals to each ring, the oxazolone ring was selectively hydrolyzed. Unfortunately, hydrolysis of the oxazolone ring resulted in the loss of all visible-CD properties above 300 nm for acid hydrolyzed mb-SB2 (Fig. 4A and 5). The visible absorbance maximum associated with the imidazolone ring (387 nm) was not affected by this treatment suggesting the CD bands in this region results from the dipolar interaction between the rings. New CD bands in the visible-CD occur following the binding of Cu^{2+} (Fig. 5A) or Hg^{2+} (Fig. 5B) and allows assignment of the CD maxima at 300 and 380 nm to the imidazolone ring and the 343 nm to the oxazolone ring.

The addition of Cu^{2+} (Fig. 4B) or Hg^{2+} (Fig. 4C) results in an increased molar ellipticity as well as the development of coupled oscillators or an exciton couple suggesting dimer formation [33 – 35]. Consistent with dimer formation, the maximal change in the CD spectra is observed at a molar ratio of 0.5 to 0.7 metal per mb-SB2 followed by a decrease, suggesting dimer dissociation (Fig. 4E and 4F). Comparison of the CD spectra following addition of CuCl2 (Fig. 4B), $HgCl_2$ (Fig. 4C) and CH_3HgCl (Fig. 4D) suggest; (1) the rotation following Cu^{2+} and Hg^{2+} binding are in opposite directions and (2) the conformational changes following CH_3HgCl additions were comparatively minor (Fig. 4D). Previous studies on mb-OB3b demonstrated the metals that are coordinated by both rings, involves a two-step mechanism, the first step involves metal binding to one ring followed by a conformational change then coordination to the second ring [9]. On the other hand, metals that bind to only one of the rings show comparatively minor conformational changes as determined by the CD spectra following metal additions. The CD spectra following CH_3Hg+ binding by mb-SB2 shows a similar trend to metals that bind to only one ring, again suggesting the imidazolone group is not involved in CH_3Hg^+ coordination to mb-SB2.

Isothermal titration calorimetry (ITC).

Of the forms of mercury examined, only $Hg(CN)_2$ fit directly as two-site model (Table 1; Fig. 6D). The $Hg(CN)_2$ titration also differed from the other mercury titrations in that the second binding site was endothermic. Both results were unexpected, since mb-SB2 does not bind CN- as measured by ITC nor were any changes observed in the UV-visible absorption or fluorescence spectra following CN- addition suggesting little to no

coordination of CN- to mb-SB2. Again, the results suggest mb-SB2 binds $Hg(CN)_2$ or one of the Hg-CN complexes and not the dissociated Hg^{2+}.

CH_3HgCl also fit a two-site model (Fig. 6), however, the CH_3HgCl titrations never moved back to zero as it approached equilibrium, at equilibrium each titration remained exothermic. The heat of dilution due to the mixing of the organic and aqueous phases was accounted for before attempting to fit the data as was the addition of CH_3HgCl in 4% methanol solution to H2O. However, a consistent thermodynamic change remained after reaching a molar ratio of 2:1 CH_3HgCl to mb-SB2 (Fig 4C). The residual heat may be a consequence of the high affinity thiol groups for CH_3Hg^+ [38]. CH_3Hg^+ has also been shown to bind to carboxyl and amine groups after all of the thiol groups are occupied [38]. Mb-SB2 has two enethiol groups and 2 CH_3Hg^+ per mb-SB2 is required before the residual thermodynamic stabilized, whereas the equilibrium for both $HgCl_2$ and $Hg(CN)_2$ was reached at 0.5 (Fig. 6). However, association to the thiol groups does not account for the consistent change in heat content as the ratio of CH_3Hg^+ per mb increased above 2.0. The consistent thermodynamic change per injection may result from a CH_3Hg^+ ligand exchange with the already bound CH_3Hg-S-R [39]. This potential ligand exchange would also account for the decreased thermodynamic change at higher CH_3Hg^+. As described in Materials and Methods, the entire data curve was shifted along the y-axis by 2000 calorie per mole in order to fit the CH_3HgCl into a two-site model. Following this shift, the enthalpy (ΔH) values were corrected by the magnitude of the shift before calculating the Gibbs free energy (ΔG). Data from $HgCl_2$ was more complex and suggested a three or four-site binding model. This complexity made fitting of the

data to particular segments of the $HgCl_2$ curve possible. Segments of the titration curves that could not be fit are listed as unable to fit (UTF) (Table 1).

Kinetics of Cu^{2+} and Hg^{2+} binding

The time course for the binding of Cu^{2+}, Hg^{2+} and $Hg(CN)_2$ to the oxazolone and imidazolone rings in mb-SB2 were measured as the decrease in absorbance at 341 and 389 nm, respectively, following stopped-flow mixing of mb-SB2 with Cu^{2+} or Hg^{2+}. The reaction was monitored at 4º C, since at 25º C less than 10% of the total absorbance change remained following stopped-flow mixing of the reaction mixture (1.4 ms). However, even at 4º C, initial binding rates could only be determined to the oxazolone ring for sub-stoichiometric concentrations of Cu^{2+} (Fig 7, table S2). The remaining binding rates for both Cu^{2+}, Hg^{2+} and $Hg(CN)_2$ to either the oxazolone ring or to the imidazolone ring were over 85% complete before 1.5 ms.

Metal binding in the presence of both Cu^{2+} and Hg^{2+}

To determine if mb-SB2 bound Hg^{2+}, Hg(CN)2 (or one of its dissociated forms) or CH_3Hg^+ in the presence of Cu^{2+}, mb-SB2 was incubated in the presence of both metals at different mercury to copper to mb-SB2 molar ratios. Preliminary analysis via UV-visible absorption spectroscopy indicated mb-SB2 does not bind $Hg(CN)_2$ or CH_3Hg^+ in the presence of Cu^{2+}. However, UV-visible absorption as well as copper and mercury analysis of the metals bound to mb-SB2 in the presence of both Cu^{2+} and Hg^{2+} demonstrated the binding of both metals (Fig. 8). At sub-stochiometric concentrations of Cu^{2+} and Hg^{2+} mb-SB2 showed a slight preference for Cu^{2+}. However, at Cu^{2+} and Hg2

to mb-SB2 at or above saturation, mb-SB2 preferentially bound Hg^{2+} over Cu^{2+} (Fig. 8). The capacity to bind Hg^{2+} in the presence of Cu^{2+} was also reflected in the reduction of Hg toxicity to *M. trichosporium* OB3b (Fig. S4)

Metal displacement

Based on the results from the mixed metal experiments, the capacity of mercury compounds to displace metals bound to mb-SB2 was examined. Hg^{2+}, $Hg(CN)_2$ and CH_3Hg^+ was found to displace Fe^{3+}, Co^{2+}, Ni^{2+}, Zn^{2+}, and Pb^{2+}. Hg^{2+} was also found to displace Cd^{2+}, Ag^+ and Cu^{2+} from mb-SB2 (Table 2). The displacement of Cu from mb-SB2 was surprising considering the high binding constant for Cu^{2+} [11]. To determine the rate of displacement, the decrease in absorbance at 324 nm after stopped-flow mixing of Cu-mb-SB2 with Au(III) at 4^o C was measured (Fig. S5). The displacement showed an initial fast rate, 118 ± 0.2 sec-1, representing 25% of the total reaction followed by a slow rate of 1.6 ± 0.1 sec-1.

Discussion

Methanobactin appears to be a copper acquisition systems used by many AMOB [1, 2, 19]. Consistent with its role in copper acquisition, the Cu binding constants for both mb-OB3b and mb-SB2 are > 1021 M [10, 11]. In addition to Cu, mb-Ob3b has been shown to bind a variety of metals including Hg [18, 19]. Recent studies have also demonstrated that mb-OB3b will reduce the toxicity of Hg to the host organism as well as to other bacterial species tested even in the presence of Cu [19]. In this report, we show the mb from *Methylocystis* strain SB2 also binds the common forms of Hg found in the

environment. Structurally, mb-OB3b and mb- SB2 occupy the extreme forms of methanobactin. Mb-OB3b is structurally the most complex chalkophore examined to date. In addition to the metal coordinating oxazolone rings, mb-OB3b is characterized by presence of the metal coordinating and redox active amino acids, Met, Tyr and Cys, and the two oxazolone rings are separated by 5 amino acids.

Mb-SB2 is a much simpler molecule, the oxazolone and imidazolone rings are separated by only two amino acids, and the reactive amino acids found in mb-OB3b are either missing or replaced with Ala. Thus, examination of the metal binding properties of mb-SB2 provides a means to evaluate the role of the two heterocyclic rings and associated enethiols in metal coordination and reduction without the complexity associated with the redox active and metal binding amino acids found in mb- OB3b. Previous comparisons in Cu^{2+} between mb-OB3b and mb-SB2 showed similar Cu binding properties [10, 11]. The results presented here also suggest that the capacity to bind different forms of mercury is a common property of chalkophores. However, in contrast to the Cu binding properties these two forms of methanobactin show different mercury binding properties. Regardless of the Hg: Cu: mb-OB3b molar ratio, the Hg to Cu molar ratio bound by mb-OB3b never exceeded 0.1 Hg to 1 Cu. Mb-SB2 on the other hand showed a Hg to Cu molar ratio between 0.5 to 6 depending on the Hg: Cu: mb-SB2 ratio. Also in contrast to mb-OB3b, Hg^{2+} was shown here to displace Cu from copper containing mb-SB2 and the displacement rate suggested an active process.

The results presented here also suggest AMOB may play a role in controlling the bioavailability of Hg and, as a result, influence the microbial community by remediating or lowering Hg toxicity to the general community. Hg binding by mb is intriguing

considering AMOB are generally present in most environments containing methane and oxygen and are probably present at Hg contaminated sites.

One unexplained observation is the mercury-induced increased fluorescent emissions of mb-SB2. Increased emission was observed following Cu^{2+} addition to mb-SB2, however, the increase was comparatively small [11]. Increased emissions are often observed following the physical disruption of two closely associated chromophores where exciton transfer occurs. [30 – 42]. In contrast to mb-OB3b, the only chromophores in mb-SB2 are the imidazolone and oxazolone rings. If internal quenching does occur, elimination of the oxazolone ring should increase emission from the imidazolone ring, which is what was observed in this study.

However, increased emissions from the imidazolone ring continued following mercury addition even in the absence of the oxazolone ring suggesting an additional mechanism is involved for the increased emissions following mercury addition. Unfortunately, this second mechanism could not be determined from the data collected.

The results presented here also demonstrate that the binding of mercury compounds by methanobactin is a function of the heterocyclic rings and associated enethiols. The rest of the molecule appears to only provide the structure to coordinate the metal binding rings and enethiol groups in an appropriate conformation. However, the structural differences between mb-SB2 and mb-OB3b appear to influence the mechanism of coordination and kinetics of binding. For example, mb-SB2 shows a greater capacity to bind Hg^{2+} in the presence of copper than does mb-OB3b [19]. On the other hand, only the oxazolone ring and the two enethiols in mb-SB2 appear capable of binding CH_3Hg^+, whereas both oxazolone rings and enethiols of mb-OB3b are involved in CH_3Hg^+

coordination [19]. The inability of the imidazolone ring in mb-SB2 to coordinate CH_3Hg^+ may reflect the overall structural differences between the two methanobactins, but the results presented here suggest the difference is due to the inability of the imidazolone ring to coordinate CH_3Hg^+. Three types of rings have been identified in the five structurally characterized methanobactins [3, 5 – 8], oxazolone, imidazolone and pyrazinedione rings, and the results presented here indicate the different rings may confer different properties to the molecule.

Conclusions

The data presented in this report demonstrates that structurally different forms of methanobactin, mb-OB3b and mb-SB2, bind both inorganic and organic forms of mercury and that the binding properties are solely dependent on the two rings and associated enethiol. However, the results also demonstrate that in contrast to mb-OB3b, mb-SB2 will preferentially bind Hg^{2+} over Cu^{2+}. The results suggest the structurally more ridged and complex mb-OB3b is a more selective Cu^{2+} binding molecule. Mb-SB2, on the other hand, behaves more like the copper-binding protein metallothionein [26], and will preferentially bind other metals such as Hg over Cu. The preferentially binding of Hg, suggest the enethiol groups in mb-SB2 may serve a more prominent role in metal binding than observed in mb-OB3b.

In addition to the environmental implications in the binding of toxic metals, the capacity to bind toxic metals may also have medical applications. In rat models, mb-OB3b has been shown to be an effective treatment for Wilson disease, a genetic defect in the copper-transporting ATPase7B resulting in copper accumulation and liver failure [44,

45]. Intravenous application of methanobactin results in the prompt release of copper from the liver into the bile [41]. Based on the results presented here, methanobactin, especially mb-SB2, may prove an effective treatment for mercury poisoning.

Abbreviations

Cu-mb-OB3b	Copper containing methanobactin from *M. trichosporium* OB3b
Cu-mb-SB2	Copper containing methanobactin from *Methylocystis strain* SB2
ITC	Isothermal titration calorimetry
mb	methanobactin
mb-OB3b	methanobactin from *M. trichosporium* OB3b
mb-SB2	methanobactin from *Methylocystis* Strain SB2
NMS	Nitrate mineral salts

Acknowledgements

We thank V. Frasca at GE Microcal for assistance in modeling the ITC results. This research was supported by the Office of Science (BER), U.S. Department of Energy (JDS and ADS) and the National Science Foundation (CHE10112271)(ADS) . Use of the ITC and stopped-flow systems were made possible through a generous gift from the Roy J Carver Charitable Trust (Muscatine, Iowa).

References

[1] J.D. Semrau, A.A. DiSpirito, S. Yoon. FEMS Microbiol. Rev. 34 (2010) 496 – 531 DOI: 10.1111/j.1574-6976.2010.00212.x.

[2] J.D. Semrau, S. Jagadevan, A.A. DiSpirito, A. Khalifa, J. Scanlan, B.Bergman, B.C. Freemeir, B.S. Baral, N.B. Bandow, A. Vorobev, D.H. Haft, S. Vuilleumier, J.C. Murrell Environ. Microbiol. 15 (2013) 3077-3086. DOI:10.1111/1462-2920.12150

[3] B.D. Krentz, H.J. Mulherron, J.D. Semrau, A.A. DiSpirito, N.L. Bandow, D.H. Haft, S.Vuilleumier S, J.C. Murrell, M.T. Mc.Ellistrem, S.C. Hartsel, W.H. Gallagher. Biochemistry 49 (2010) 10117-10130.

[4] G.E. Kenny and A.C. Rosenzweig. *BMC Biology* 11 (2013) 17. DOI: 10.1186/1741-7007.

[5] H.J. Kim, D.W. Graham, A.A. DiSpirito, D. Alterman, M.A.N.Galeva, C.K. Larive, D. Asunskis. P. Sherwood. Science 305 (2004) 1612 – 1615. DOI: 10.112.

[6] A. El Ghazouani, A. Baslé, S.J. Firbank, C.W. Knapp, J. Gray, D.W. Graham, C. Dennison. Inorg. Chem. 50 (2011) 1378 – 1391. DOI: 10.1021/ic101965.

[7] A. El Ghazouani, A. Baslé, J. Gray, D.W. Graham, S.J. Firbank, C. Dennison. Proc. Natl. Acad. Sci. USA. 109 (2012) 8400 – 8404. DOI: 10.1073/pnas.1112921109.

[8] L.E. Behling, S.C. Hartsel, D.E. Lewis, A.A. DiSpirito, L.R. Masterson, G. Veglia, W.H. Gallagher. J. Am. Chem. Soc.130 (2008) 12604 – 12605 DOI: 10.1021/ja804747d.

[9] D.W. Choi, Y.S. Do, C.J. Zea, M.T. McEllistrem, S.W. Lee, J.D. Semrau, N.K. Pohl, C.J. Kisting, L.L.Scardino, S.C. Hartsel, E.S. Boyd, G.G. Geesey, P.H. Shafe, T.P. Riedel, K.A. Kranski, J.R. Tritsch, W.E. Antholine, A.A. DiSpirito. J. Inorgan. Biochem. 100 (2006) 2150– 2161 DOI: 10.1016/j.inorgbio.2006.08.017.

[10] D.W. Choi, C.J. Zea, Y.S. Do, J.D. Semrau, W.A. Antholine, M.S. Hargrove, Pohl NL, E.S. Boyd ES, G.G. Geesey, S.C. Hartsel, P.H. Shafe PH, M.T. McEllistrem, C.J. Kisting, D. Campbell, V. Rao V, A.M. de la Mora AM, A.A. DiSpirito. Biochemistry. 45 (2006) 1142 – 1153.

[11] N. Bandow, V.S. Gilles, B.C. Freesmeier, J.D. Semrau, B. Krentz, W.H. Gallagher, M.T. McEllistrem, S.C. Hartsel, D.W. Choi, H.S. Hargrove, T.M.

Heard, L.M. Chesner, K.M. Braunreiter, B.V. Cao, M.M. Gavitt, J.Z. Hoopes, J.M. Johnson, E.M. Polster, B.D. Schoenick, A.M. Umlauf, A.A. DiSpirito. J. Inorg. Chem. 110 (2012) 72– 82. DOI: 10.1016/j.jinorgbio.2012.02.002.

[12] D.W. Choi , J.D. Semrau, W.E. Antholine, S.C. Hartsel, R.C. Anderson, J. Carey, A.M. Dreis, E.M. Kenseth, J.M. Renstrom JM, L.L. Scardino, G.S. Van Gorden, A.A. Volkert, A.D. Wingad, P.J. Yanzer PJ, M.T. McEllistrem, A.M. de la Mora, A.A. DiSpirito. J. Inorg. Biochem. 102 (2008) 1571 – 1580. DOI: 10.1016/j.inorgbio.2008.02.003.

[13] D.W. Choi, W.A. Antholine, Y.S. Do, J.D. Semrau, C.J. Kisting, R.C. Kunz, D. Cambel, V. Rao, S.C. Hartsel, A.A. DiSpirito AA. Microbiology 151 (2005) 3417 - 3426. DOI: 10.1099/mic.0.28169-0

[14] J.A. Zahn, A.A. DiSpirito. J. Bacteriol. 178 (1996) 1018 - 1029. DOI: 10.1128/JB.185.19.5755-5764.2003 J. Bacteriol.

[15] C.M. Tellez, K.P. Gaus, D.W. Graham, R.G. Arnold, R.Z. Guzman RZ Appl. Environ. Microbiol. 64 (1998) 1115 – 1122.

[16] N.L. Bandow, W.H. Gallager, L. Behling, D.W. Choi, J.D. Semrau, S.C. Hartsel, V.S. Gilles VS, A.A. DiSpirito. Meth. Enzymol. 495 (2011) 260 – 269.

[17] S. Yoon, S.M. Kraemer, A.A. DiSpirito, J.D. Semrau JD. Environ. Microbiol. 2 (2010) 295- 303.

[18] S. Yoon, A.A. DiSpirito, S.M. Kraemer, J.D. Semrau JD. Meth. Enzymol. 495 (2011) 248- 259.

[19] A. Vorobev, S. Jagadevan, B.S. Baral, A.A. DiSpirito, B.C. Freemeier, B.H. Bergman, N.L. Bandow, J.D. Semrau. Appl. Environ. Microbiol. 79 (2013) 5918 – 5926. DOI: 10.1128/AEM.01673-13.

[20] R. Whittenbury, K.C. Phillips, J.F. Wilkinson JF. *J Gen Microbiol* 61 (1070) 205-218.

[21] O.H. Lowry, N.J. Rosebrough, A.I. Farr, R.J. Randall. J. Biol. Chem. 193 (1951) 265 – 275.

[22] F. Takeuchi, A. Negishi, T. Maeda, K. Kamimura, T. Sugio. J. Biosci. Bioeng. 95 (2003) 239 – 244.

[23] M. Vasàk, J.H. Kägi, H.A.O. Hill HAO. Biochemistry 20 (1981) 2852-2856.

[24] K.B. Nielson, D.R. Wingel DR. J. Biol. Chem. 258 (1983) 13063 – 13069

[25] J.H. Kägi, B.L. Vallee, J.M Carlson. J. Biol. Chem. 236 (1961) 2435 – 2442.

[26] K.B. Nielson, C.L. Atkin, D.R. Winge DR. J. Biol. Chem. 260 (1985) 5342 – 5350.

[27] G.K. Carson, P.A.W. Dean, M.J. Stillman MJ. Inorgan. Chim. Acta. 56 (1981) 59 – 71.

[28] W.M. Lattamer, J.H. Hildebrand JH. Reference Book of Inorganic Chemistry (1940) The Macmillian Co., NY.

[29] M.T. Beck MT. Pure Appl. Chem. 59 (1987) 1703 – 1720.

[30] M. Kaup, H.G. Schnering HG. Inorg. Chem. 33 (1994) 4718 – 4722. DOI: 10.1021/k00099a23

[31] S. Georgakopoulou, R. Grondelle, D. van der Zwan. Biophys. J. 86 (2004) 3010 – 3022. DOI: 10.152.biophysj.104.047-498.

[32] S. Georgakopoulou, R. Grondelle, D. van der Zwan. J. Phys. Chem. B. 110 (2006) 3344 – 3353. DOI: 10.1021/jp051794c.

[33] E.H. Strickland D. Mercola. Biochemistry 15 (1976) 3875 – 3884.

[34] J. Goldman F.H. Carpenter FH. Biochemistry 13 (1974) 4566 – 4574.

[35] S. Superchi, E. Giorgio, C. Rosini C . Chirality 16 (2004) 422 – 451.

[36] J. Seibt, A. Lohr A, F. Würthner, V. Engel. Phys. Chem. Chem. Phys. 9 (2007) 6214 – 6218.

[37] A. Amirbahman, A.L. Reid, T.A. Haines, J.S. Kahl, C. Arnold C. Environ Sci Technol 36 (2002) 690-695.

[38] S. Yoon, L.M. Diener, P.R. Bloom, E.A. Nater, W.F. Bleam WF. Geochim. et Cosmochim. Acta. 69 (2005) 1111-1121.

[39] D.J. Rabenstein. R.S. Reid RS. Inorg. Chem. 23 (1984) 1246-1250.

[40] G.M. Vandal, W.F. Fitzgerald, K.R. Rolfnus, C.H. Lamborg. Water Air Soil Pollut. 80 (1995) 5929 – 528.

[41] J. Ye, K. Sun, Y. Zhao, Y. Yu, C.K. Lee, J. Cao. J. Chem. Phys. 136 (2012) 245104 – 24518.

[42] A. Stirbet. Photosynth. Res. 116 (2013) 189 – 214. DOI: 10.1007/s/11120-013-9863-9.

[43] A. Freer, S. Prince, K. Sauer, M. Papiz, A. Hawthornthwaite-Lawless, G. McDermott, R. Cogdell, N.W. Isaacs NW. Structure 4 (1996) 449 – 462.

[44] K.H. Summer, J. Lichtmannegger, B. Michalke, N.L. Bandow, D.W. Choi, A.A. DiSpirito, B. Michalke B. J. Trace Elem. Med. Biol. 25 (2011) 36 - 41. DOI: 10.1016/j.jtemb.2010.12.002.

[45] H. Zischka, J. Lichtmannegger, S. Schulz, S. Schmitt, N. Jägemann, D. Hamöller, L. Jennen, C. Rust, N. Larochette, L. Galluzzi, V. Chajes, N.L. Bandow, V.S. Gilles, A.A. DiSpirito, I. Esposito, M. Goettlicher, K.H. Summer, G. Kroemer G. J. Clin. Investigation. 121 (2011) 1508 – 1518. DOI:10.1172/JCI45401.

Figures

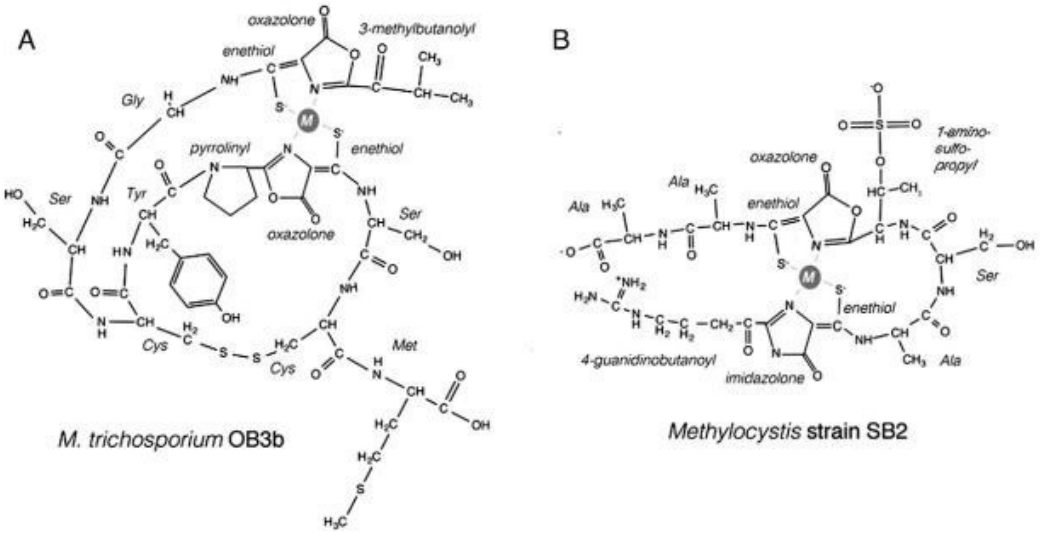

Figure 1. Chemical structures of methanobactin from *M. trichosporium* OB3b (A) and from *Methylocystis* strain SB2 (B).

Abbreviation: M, metal that is coordinated by both rings and enethiol groups of methanobactin.

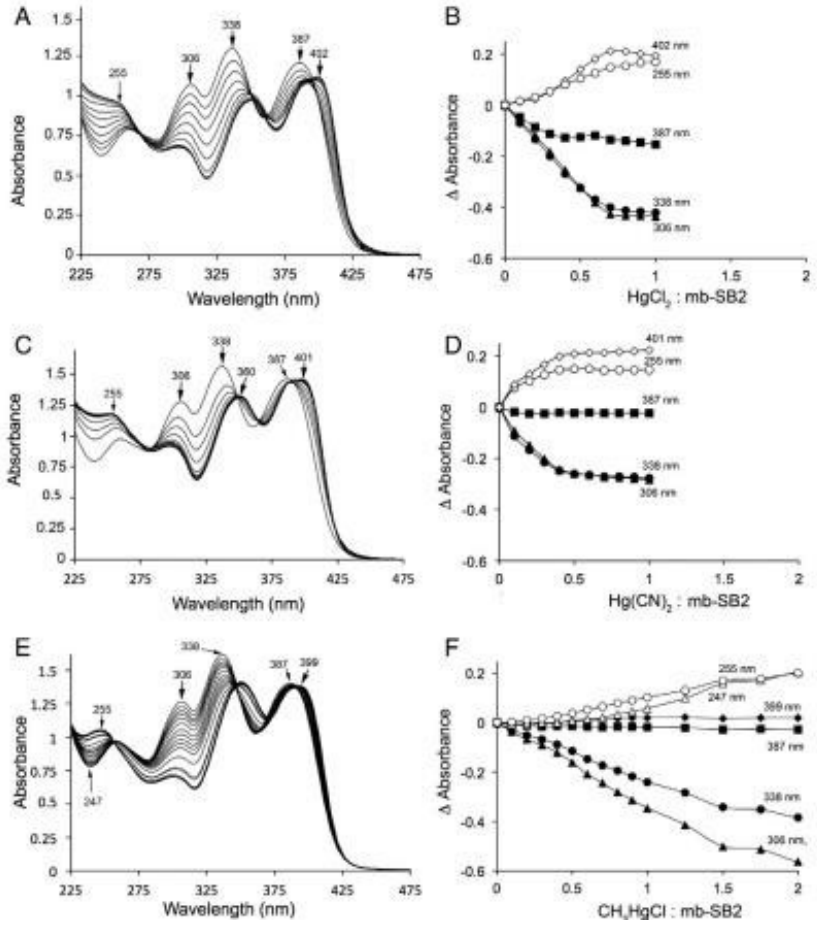

Figure 2. UV-visible absorption spectra of mb-SB2 as isolated and following the addition $HgCl_2$ (A and B), $Hg(CN)_2$ (C and D) or CH_3ClHg (E and F). Absorbance changes at 247 (△), 255 (○), 306 (▲), 338 (●), 387 (■), 399 (◆) and 402/401 nm (◇) following the addition of $HgCl_2$ (B), $Hg(CN)_2$ (D), or CH_3HgCl (F).

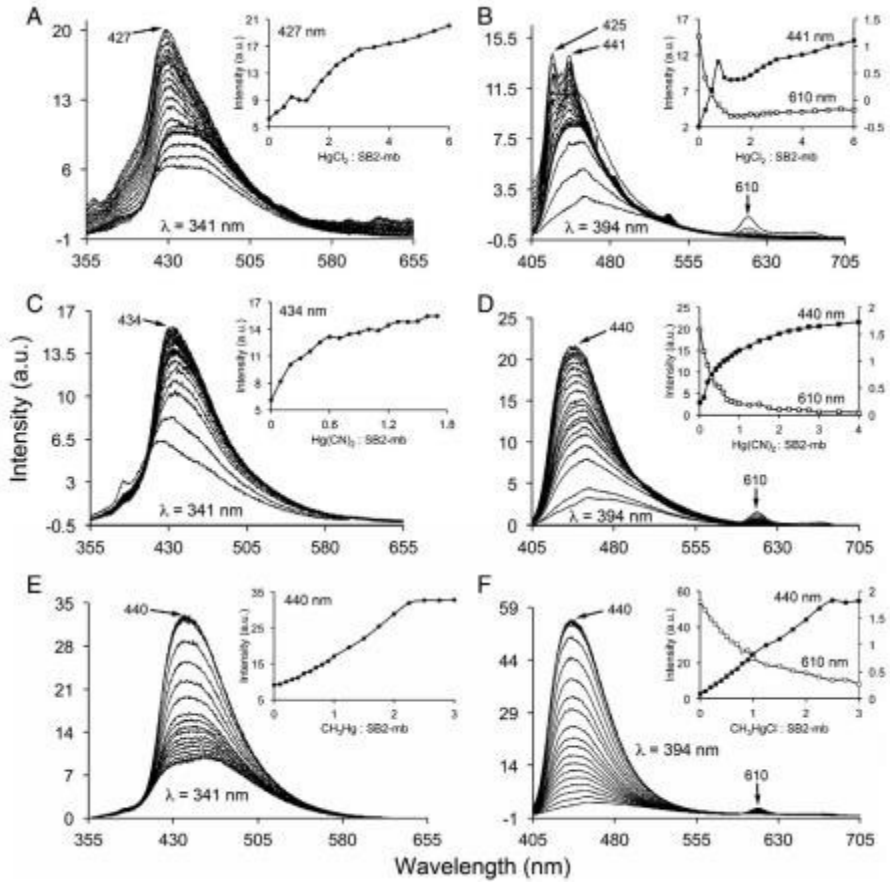

Figure 3. Emission spectra from mb-SB2 following excitation at 341 (A, C and E) 394 nm (B, D and F) as isolated and following the addition of $HgCl_2$ (A and B), $Hg(CN)_2$ (C and D), or CH_3HgCl (E and F . Inserts emission intensities at 427 (A), 434 (C) or 440 (●) and following excitation at 341 nm and at 441 or 440 (■) and 610 (□) following excitation at 394 nm (B, D, and F).

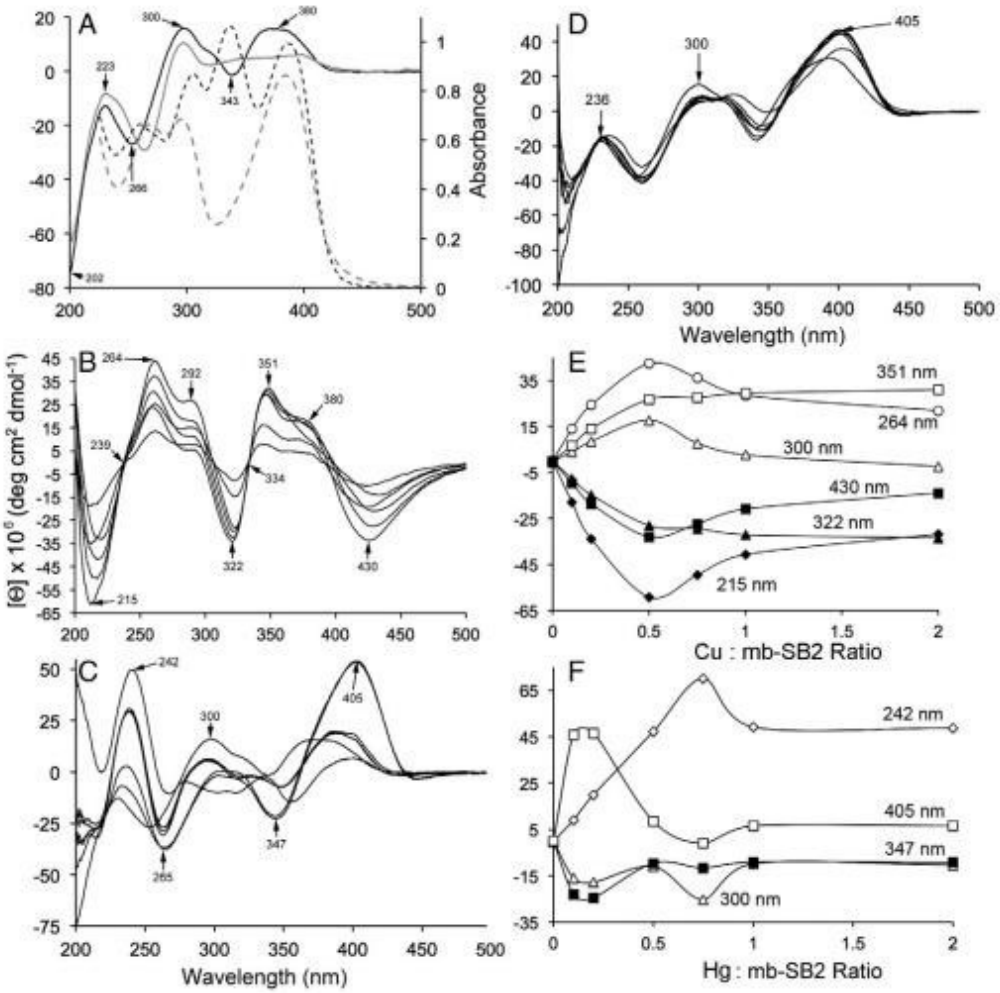

Figure 4. (A) UV-visible absorption (— —; — —) Cirular dichroism (——; ——) spectra of mb-SB2 as isolated (— —; ——) and following acid hydrolysis of the oxazolone ring (— —; ——) UV-visible circular dichroism of mb-SB2 as isolated and following the addition of (B) 0.1, 0.2, 0.5 0.75, 1.0 and 2.0 $CuCl_2$; (C) 0.2, 0.5, 0.75, 1.0 and 2.0 $HgCl_2$; and (D) 0.2, 0.5, 0.75, 1.0 and 2.0 CH_3HgCl per mb-SB2. (E) Change in molar ellipticity at 215 (◆), 264 (○), 300 (△), 322(▲), 351 (□), and 430 (■) nm following the addition of $CuCl_2$. Change in molar ellipticity at 242 (◇), 300 (△), 347 (■), and 405 (□) nm following the addition of $HgCl_2$.

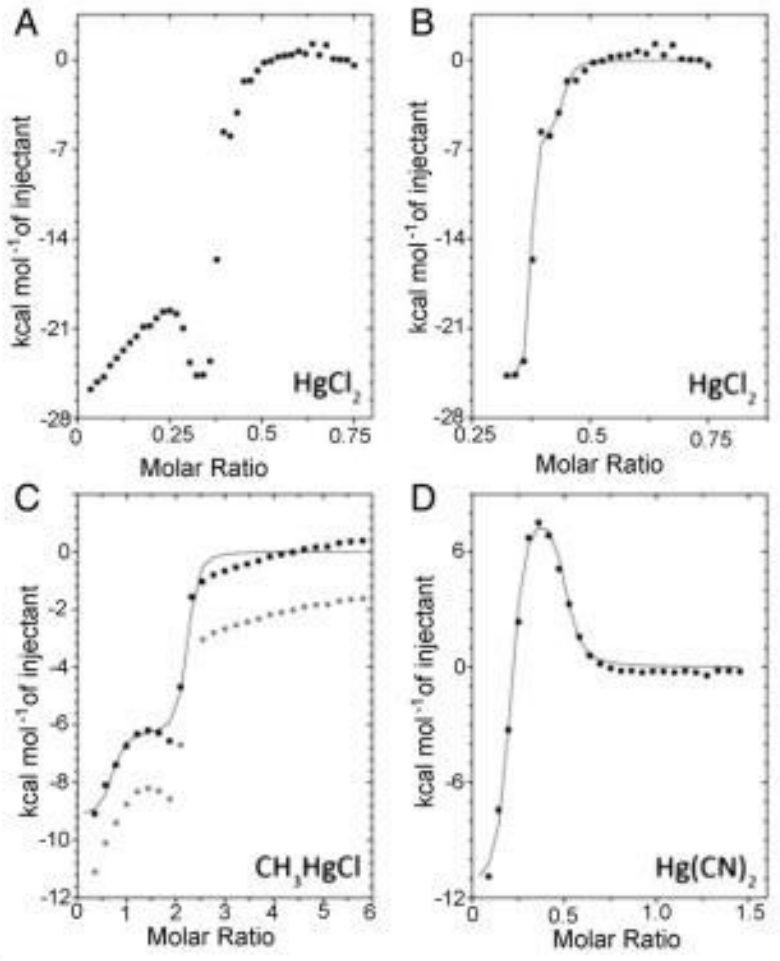

Figure 5. A. Binding isotherm following the addition of $HgCl_2$ to mb-SB2. B. The binding isotherms for the second and third binding sites of $HgCl_2$ of mb-SB2. C. The binding isotherm following the addition of CH_3HgCl to mb-SB2 (●) and following a 2000 cal per mole adjustment to the binding isotherm (●). D. The binding isotherm following the addition of $Hg(CN)_2$ to mb-SB2. The solid lines in pannels B, C and D shows the curve fitting for a two-site binding algorithm..

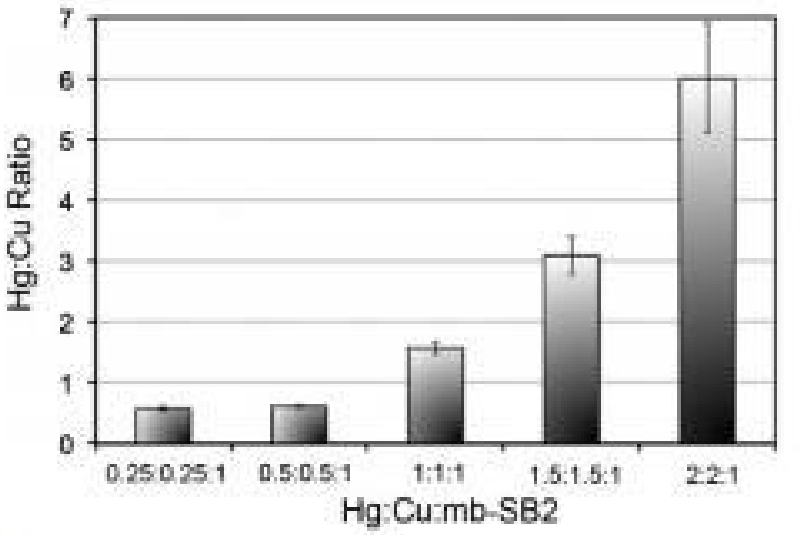

Figure 6. Ratio of Hg to Cu bound to mb-SB2 following incubaction of the mb-SB2 in solutions containing Cu^{2+}, Hg^{2+} and mb-SB2 in molar ratios of 0.25:0.25:1, 0.5:0.5:1, 1:1:1, 1.5:1.5:1, and 2:2:1, respectively.

Tables

Table 1
Thermodynamic parameters for $HgCl_2$, $Hg(CN)_2$ and CH_3ClHg binding to mb-SB2 at 25 °C.

Parameter	$HgCl_2$	CH_3HgCl	$Hg(CN)_2$
N_1 (Hg mb-SB2^{-1})	UTF[†]	0.62	0.19
K_1 (M^{-1})	UTF	1.2×10^8	7.5×10^7
ΔH_1 (cal mol^{-1})	UTF	−11,190*	−11800
ΔS_1 (cal mol^{-1} deg^{-1})	UTF	6.07	−3.55
ΔG_1 (cal mol^{-1})	UTF	−13,000*	−10,742
N_2 (Hg mb-SB2^{-1})	0.37	1.52	0.30
K_2 (M^{-1})	7.5×10^9	1.7×10^6	1.8×10^6
ΔH_2 (cal mol^{-1})	−25,000	−8,300*	9,000
ΔS_2 (cal mol^{-1} deg^{-1})	−38.7	7.4	58.8
ΔG_2 (cal mol^{-1})	−13,462	−10,506*	−8,531
N_3 (Hg mb-SB2^{-1})	0.07	–	–
K_3 (M^{-1})	6.87×10^6	–	–
ΔH_3 (cal mol^{-1})	−5800	–	–
ΔS_3 (cal mol^{-1} deg^{-1})	11.8	–	–
ΔG_3 (cal mol^{-1})	−9318	–	–
χ^2	8.36×10^5	1.48×10^5	2.04×10^5

*Calculated values following a 2000 cal mol^{-1} shift.
† UTF, unable to fit.

CHAPTER 3

KINETICS AND SPECTRAL PROPERTIES OF $AUCL_4^-$ BINDING BY METHANOBACTIN: EVIDENCE FOR THE TETRAMER, DIMER, MONOMER MODEL

Erick A. Turpin*, Bipin S. Baral*, Nathan L. Bandow, Jeremy D. Semrau, and Alan A. DiSpirito

* These authors contributed equally to the manuscript

Abstract

Methanobactins (mbs) are small post-translationally modified copper-binding polypeptides produced by many methanotrophic bacteria. In this report, $AuCl_4^-$ binding by mb from *Methylocystis* strain SB2 (mb-SB2) was measured and compared to $AuCl_4^-$ binding by the mb from *Methylosinus trichosporium* OB3b (mb-OB3b). The UV-visible absorption, fluorescent and circular dichroism spectral changes following $AuCl_4^-$ titrations in mb-SB2, supports the tetramer, dimer and monomer model previously proposed for Cu^{2+} binding by mb-OB3b. The kinetic properties of $AuCl_4^-$ binding by mb-SB2 were comparable to that of Cu^{2+} binding, with initial bind to the imidazolone ring complete in less than 1.4 ms at 4° C. Binding to the oxazolone ring was slower and showed a non-Michaelis-Menten dependence on the $AuCl_4^-$ concentration.

At 4° C, $AuCl_4^-$ binding to both oxazolone rings could be monitored in mb-OB3b. In contrast to Cu^{2+}, which initially binds to oxazolone A, $AuCl_4^-$ initially bound to the oxazolone B moiety, followed by a lag time of 1.6 to 134 ms, depending on the $AuCl_4^-$ to mb-OB3b ratio, before the initial coordination to the oxazolone A group. Exciton transfer between the two- oxazolone rings was disrupted during the lag period with an associated increase in absorption by oxazolone A. Pre-steady state kinetics for mb-OB3b also supported the tetramer, dimer, monomer model for metal binding.

Introduction

Methanobactins (mbs) are small (<1,200 Da) post-translationally modified polypeptides produced by many, but not all, aerobic methane-oxidizing bacteria or methanotrophs [1-6]. The molecule is the first characterized example of a chalkophore, i.e., a compound excreted by bacteria to scavenge copper from the surrounding environment [1]. Structurally, mbs are characterized by the presence of one oxazolone ring and a second ring five or six membered ring separated by 2-5 amino acids [1-5]. The second ring is either an oxazolone, an imidazolone, or an pyrazinedione ring. Each ring is associated with a thioamide group, which together form the metal coordination site.

Structurally, mbs can be divided into two groups. One group is represented by the mb from *Methylosinus trichosporium* OB3b (mb-OB3b). In addition to the core properties listed above, mb-OB3b contains a pyrrolidinyl group, one Met, one Tyr, one Gly, two Ser, and two Cys residues that form a stable intermolecular disulfide bond that provides a compact pyramid-like structure with the metal coordination site at the base [1,3,6]. The second group is represented by mbs from *Methylocystis* strains. These are smaller, < 900 Da, simpler and less rigid molecules [2,4]. For example, in addition to the core properties, mb from *Methylocystis* strain SB2 (mb- SB2) consists of three Ala residues, one Ser residue, a guanidinobutanyl and a sulfate group. Thus, a comparison of the metal binding properties of mb-OB3b and mb-SB2 should provide insight into the role(s) of the peptide backbone in metal binding and reduction properties of chalkophores.

In addition to copper, both mb-OB3b and mb-SB2 have been shown to bind several transition and near transition metals [5,7-10]. With the exception of Ag^{+}, Pb^{2+}, Hg^{2+} and $AuCl_4^{-}$, the binding constants are several orders of magnitude below those observed for copper and Cu^{2+} will displace most other metals previously bound to mb-

OB3b. Considering the structural differences between mb-SB2 and mb-OB3b, the question of whether different types of mb show different metal binding characteristics has yet to be investigated in depth. A recent study demonstrated that in contrast to mb-OB3b, mb-SB2 preferentially binds Hg^{2+} over Cu^{2+} and that the mercury binding properties of mb-SB2 differs from those observed with mb-OB3b [8,10]. In this report we examined the $AuCl_4^-$ binding properties of mb-SB2 and mb-OB3b. The results demonstrate that the peptide backbone does influence metal binding by mb.

Results and Discussion

UV-visible absorption

The UV-visible absorption spectra changes following $HAuCl_4$ addition suggest $AuCl_4^-$ binds to oxazolone (334 nm) and imidazolone (387 nm) rings as well as the thioamide moieties (258 nm) of mb-SB2 (Fig. 1). The spectra following the addition of $AuCl_4^-$ to mb-SB2 was complex with multiple shifts and changes from decreasing to increasing absorption with increasing $AuCl_4^-$ concentrations. The major transitions appear at approximately 0.5 (Figs. 1A), 1.0 (Figs. 1B and 1C), and > 1.0 (Fig. 1D) $AuCl_4^-$ per mb-SB2 ratios. The oxazolone and imidazolone groups both showed redshifts suggesting an in-line orientation of the transition dipoles of the ring moieties following $AuCl_4^-$ addition [11].

The spectral transitions appear to be dependent on either different oligomeric forms of mb-SB2 or to pH changes that occur during $AuCl_4^-$ titration of mb-SB2 prepared in > 18MΩ▪cm H2O. The pH initially increased from 6.95 to 7.45 at $AuCl_4^-$ to mb-SB2 ≤ 0.3, followed by a consistent decrease to 5.7 at higher $AuCl_4^-$ to mb-SB2 ratios. Like mb-OB3b (12), mb-SB2 is stable in this pH range (results not shown). Although the observed

pH changes complicates interpretation of results, the following experiments will focus on $AuCl_4^-$ and mb-SB2 solutions prepared in > 18MΩ▪cm H2O. The interaction of $AuCl_4^-$ with the buffers tested (i.e. 3-(N- morpholino)propanesulfonic acid, pH 7.3, piperazine-N, N',-bis(ethanesulfonic acid, pH 7.3, and phosphate buffer, pH 7.3) as well as the effects of buffers on the spectral properties of mb- SB2 posed more serious complications (results not shown).

Fluorescence

Emission spectra following excitation at 285 nm showed two distinct emission maxima at 305 and 426 nm (Figure 2A). The emission maxima at 305 nm decreased following $AuCl_4^-$ addition, but emission at 426 nm increased and shifted to 417 nm with major transitions at 0.5 and 1.0 $AuCl_4^-$ per mb-SB2, followed by a decrease in emission intensity at higher $AuCl_4^-$ to mb- SB2 ratios. The emission spectra following excitation at 341 nm and $AuCl_4^-$ addition showed increased emission 417 nm with a shift in the spectra to 426 nm with transitions in the titrations at 0.25, 0.5 and 1.0 $AuCl_4^-$ per mb-SB2. At $AuCl_4^-$ to mb-SB2 ratios > 1.0, the emission maximum shifted from 426 nm back to 417 nm and the emission intensity decreased to the intensity before $AuCl_4^-$ addition at 2.0 $AuCl_4^-$ per mb-SB2 (Figure 2C). A similar trend was observed following excitation at 394 nm and the addition of $AuCl_4^-$, but the major emission was at 453 nm.

Based on emission intensities, four different trends were observed during $AuCl_4^-$ titrations. Mb-SB2 has only one identified metal binding site, we therefore interpret these data to indicate changes in $AuCl_4^-$ coordination, transitioning from an oligomeric state, possibly starting as tetramer, to a dimer and finally to a monomer. The transition at $AuCl_4^-$ to mb-SB2 ratios above 1.5 appears to be associated with nanoparticle formation. The

increased emission intensity following $AuCl_4^-$ addition involves disruption of internal quenching between the imidazolone and oxazolone groups and is consistent with the intra-molecule exciton transfer previously demonstrated following hydrolysis of the oxazolone ring [13]. Consistent with intra- molecular exciton transfer, the most intense emission intensity was observed at $AuCl_4^-$ to mb- SB2 ratio of 1:1 (Figure 2A, B and C).

UV-visible circular dichroism (CD)

As previously described [8], the UV-visible circular dichroism **(**CD) spectrum for mb-SB2 as isolated corresponded to that of an unordered polypeptide, showing a strong negative band at 210 nm. At $AuCl_4^-$ at or below 0.75 $AuCl_4^-$ per mb-SB2 the absorbance at 210 nm is essentially constant (Fig. 3C), but at higher $AuCl_4^-$ to mb-SB2 ratios the signal at 210 nm becomes more positive and is close to zero at 2.0 $AuCl_4^-$ per mb-SB2 suggesting an ordered molecule.

The fluorescent spectra (Fig. 2) as well as previous spectral studies following hydrolysis of the oxazolone ring [9,13], suggest exciton transfer between the oxazolone and imidazolone rings. However, in the absence of $AuCl_4^-$, no exciton coupling was observed in the visible CD spectra between the oxazolone and imidazolone groups (Fig. 3A). Maxima ellipticity was observed from the oxazolone and imidazolone at 326 and 378 nm, but both groups showed a positive signal. The absence of exciton coupling in the visible CD spectra suggest the dipoles are inline or in a parallel arrangement. Following the $AuCl_4^-$ addition, exciton coupling was observed and with a negative exciton chirality and a new positive band at 416 nm. At molar rations between 0.1 and 0.5 $AuCl_4^-$ per mb-SB2 the amplitude between the 347 and 378 nm bands increased, followed by a decrease at higher $AuCl_4^-$ to mb-SB2 ratios (Fig. 3D). No CD transitions were observed at $AuCl_4^-$

to mb-SB2 greater than one, again suggesting the dipoles are in-line or in a parallel arrangement. Based on the redshifts in the UV-visible absorption spectra (Fig. 1), the arrangement appears to be in-line [11].

The molar ellipticity changes for mb-SB2 were greater than that observed with mb-OB3b [7] and suggest mb-SB2 can undergo much larger conformational changes than mb-OB3b. The presence of the disulfide bond found in mb-OB3b is the probable reason for this difference.

Kinetics of $AuCl_4^-$ Binding

The time course for the binding of $AuCl_4^-$ to the oxazolone and imidazolone rings in mb-SB2 was measured as the decrease in absorbance at 341 and 389 nm, respectively, following stopped- flow mixing of mb-SB2 with HAuCl4 at 4□C. Unfortunately, even at 4° C, initial binding to the imidazolone ring was complete before mixing of the sample was complete (1.4 ms), indicating binding rates greater than 1600 s-1. In contrast, initial binding rates to the oxazolone ring were low, < 60 s-1, at $AuCl_4^-$ to mb-SB2 ratios below 0.3, increased at $AuCl_4^-$ to mb-SB2 ratios between 0.3 and 1.5 $AuCl_4^-$ per mb-SB2, followed by a decline in rate at molar ratios >1.5 $AuCl_4^-$ per mb-SB2 (Fig. 4). Decreased rates of binding at molar ratios >1.5 $AuCl_4^-$ per mb-SB2 is probably the result of nanoparticle formation observed to occur at molar ratios >1.5 $AuCl_4^-$ per mb-SB2 (results not shown).

The kinetics of $AuCl_4^-$ binding by mb-OB3b were slower than to mb-SB2 and provided insight into the mechanism of metal binding by methanobactins. Previous room temperature pre- steady state kinetics of Cu^{2+} by Choi et al. [7] demonstrated Cu^{2+} initially bound to oxazolone A followed by a short, 4 – 6 ms, lag period before initial coordination

to oxazolone B [7]. Unfortunately, in that study, Cu^{2+} binding to oxazolone A was complete before the initial reading at 1.4 ms. In contrast, at 4° C, the rate of $AuCl_4^-$ binding to both oxazolone groups in mb-OB3b could be monitored. The results show that $AuCl_4^-$ initially binds to oxazolone B followed by a lag period before binding to oxazolone A (Fig. 5). The lag time before initial binding to oxazolone A varied between 1.6 and 134 ms, depending on the $AuCl_4^-$ to mb-OB3b ratio, (Fig. 6B). Exciton transfer between the two-oxazolone rings was apparently disrupted during the lag period as an increase in absorption by oxazolone A was observed before initial coordination of $AuCl_4^-$

Pre-steady state kinetics of $AuCl_4^-$ binding to both oxazolone A and B in mb-OB3b revealed a complex reaction mechanism resulting in increased as well as decreased absorbance changes by both groups. To calculate the rate constants, we assigned a decrease in absorbance to coordination of $AuCl_4^-$ and gave that value a positive sign. On the other hand, an increase in absorbance was assumed to be the result of uncoupling of the exciton transfer between the rings or decreased association to $AuCl_4^-$ and was assigned a negative value. Overall, four different binding constants could be determined, before equilibrium. Regardless of the $AuCl_4^-$ to mb- OB3b ratio, oxazolone B is solely responsible for first binding constant, k1 (Fig. 5). The minor increases in absorbance in by oxazolone A were probably the result of disruption of exciton transfer between the rings. K1 for oxazolone B showed a small decrease at $AuCl_4^-$ to mb-OB3b ratios between 0.05 and 0.25 $AuCl_4^-$ to mb-OB3b ratios then increased with increasing concentrations of $AuCl_4^-$ (Fig. 5). The transition at 0.25 $AuCl_4^-$ per mb-OB3b is consistent with the model proposing methanobactin initially binds metals as a tetramer using only one of the rings and associated thioamide [7]. Consistent with this model, the largest spectral change in oxazolone B was observed at 0.25 $AuCl_4^-$ to mb-OB3b (Fig. 6). Coordination of $AuCl_4^-$ to

oxazolone B appears be complete at this stage and subsequent decrease in absorption are associated with coordination of oxazolone A to $AuCl_4^-$ or Au^0. The final oxidation state of gold in mb-OB3b is Au^0, [7].

The second rate constant, *k2*, appears to involve the initial coordination of $AuCl_4^-$ to oxazolone A. We assume the change from *k2* to *k3* is associated with a conformation change in mb-OB3b as both rings and associated thioamides becomes involved in the coordination of $AuCl_4^-$ or Au^0. The last rate constant, *k4,* appears to be the final equilibrium between the rings and $AuCl_4^-$ or Au^0.

Metal Displacement

UV-visible absorption spectra demonstrated Cu^{2+} could not displace Au^0 from mb-SB2 (results not shown). However, $AuCl_4^-$ displaced Cu^+ pre-bound to mb-SB2 (Fig. 8A). The displacement of Cu^{2+} by Au^{3+} was unexpected and was examined in more detail. First, mb-SB2 was added to solutions containing both Au^{3+} and Cu^{2+} at different molar ratios (Figure 9). Analysis of the metals bound to mb-SB2 in these mixed metal environments demonstrated that mb-SB2 preferentially bound Au^{3+} over Cu^{2+} at molar ratios ≥ 0.5 (Figure 9). Second, the displacement rate was determined by measuring the decrease in absorbance at 324 nm following stopped-flow mixing of Cu-mb-SB2 with Au^{3+} at 4˚C, and showed an initial displacement rate of 3.45 ± 0.02s-1 (Figure 8B).

Summary and Conclusions

Studies on the metal binding properties of methanobactin have focused on copper, and in general the different forms of mb show similar copper binding properties [3,4,8,24]. In contrast, this study indicates that structurally different forms of mb can react quite

differently to other metals. Here we focus on mb-SB2, since this modified polypeptide does not contain the redox active and metal-binding groups observed in the more complex mb-OB3b. The results presented here demonstrate the structural differences between methanobactins can influence metal binding properties. Overall, the mechanism of binding and binding constants of mb-OB3b and mb-SB2 for Cu^{2+} are similar (Choi, 2006, Baral 2011). However, in contrast to mb-OB3b, mb-SB2 $AuCl_4^-$ and Hg^{2+} [17] and both metals will displace Cu^+ from Cu-mb-SB2 demonstrating either the protein backbone or type of N-terminal heterocyclic ring alters the metal binding properties of methanobactins.

Experimental Section

Organism, culture conditions and isolation of methanobactin

Methylocystis strain SB2 was cultured in 0.2 or 1.0 μM CuSO4 amended nitrate mineral salts (NMS) medium [19] in sequential batch reactors and mb-SB2 purified from the spent medium as previously described [17].

Protein and metal determination

Protein was determined by the Lowry method [20]. Samples for metal analysis were hydrolyzed for 12 h at 37º C in 0.6N HCl plus 0.6 N HNO3. Copper and gold concentrations were determined on an Agilent 55AA atomic absorption spectroscopy (Agilent Technologies Inc., Santa Clara, CA) in flame mode as previously described [17].

UV-visible absorption, UV-visible circular dichroism, and fluorescence spectroscopy

UV-visible absorption spectroscopy, and fluorescence spectroscopy scans and titrations were performed on a Cary 50 (Agilent Technologies Inc., Santa Clara, CA), and

a Cary Eclipse (Agilent Technologies Inc.), respectively. Reaction mixtures for UV-visible absorption, XPS and fluorescence spectroscopy contained 50 μM mb-SB2 and were titrated with 10 mM HAuCl4 in >18MΩ▪cm H2O, in 10 mM 3-(N-morpholino)propanesulfonic acid (MOPS), pH 7.3, in10 mM piperazine-N, N',-bis(ethanesulfonic acid (PIPES), in pH 7.3, or phosphate buffer, pH 7.3. Buffer solutions were prepared in > 18MΩ▪cm H2O. Time course UV-visible absorption spectra were performed with 50 μM mb-SB2 solutions containing 112.5 μM HAuCl4 in either, > 18MΩ▪cm H2O. Scans were taken every 5 min for 1 h or every 60 min for 48 h. For excitation fluorescence maxima, spectra were taken at a scanning rate of 30 nm sec^{-1} between 290 and 700 nm with excitation and emission slits at 5 nm and a photomultiplier tube voltage of 600 V. Excitation wavelengths of 285, 341 or 394 nm were used with spectra taken every 2.5 min.

Circular dichroism (CD) spectroscopy was performed on a JASCO J-710 spectropolarimeter (Jasco Co., Tokyo, Japan) with a 1 cm quartz cuvette. A 500 μM solution of mb-SB2 was titrated with 10 mM HAuCl4, both prepared in > 18MΩ▪cm H2O.

Kinetics of $AuCl_4^-$ binding

The rates of $AuCl_4^-$ binding to mb-SB2 and mb-OB3b were determined by measuring absorption changes at 341 nm and 389 nm using a four-syringe Biologic SFM/4000/S stopped flow reactor coupled to a MOS-500 spectrophotometer (Bio-Logic Science Instrument SA, Claix, France) at 4° C as previous described [17]. In contrast to the absorbance maxima using Cary 50 spectrometer, the absorbance maximum for the oxazolone and imidazolone rings were 341 and 389 nm, respectively, on this system. Stock solutions of HAuCl4 were prepared in >18MΩ▪cm H2O. The stock solutions of mb-

SB2 were prepared by dissolving freeze-dried mb-SB2 in >18MΩ▪cm H2O. For Cu-mb-SB2, CuSO4 was added to mb-SB2 in molar ratios of 1 Cu^{2+} per mb-SB2. Stock solutions of HAuCl4, mb-SB2 and Cu-mb-SB2 were chilled on ice then filtered through 0.22 µm filter before loading into sample syringes. Final concentration of the stock solutions of mb-SB2 and Cu-mb-SB2 were determined after filtration by UV-visible absorption spectroscopy as previously described [10,16]. Path length for the cuvette used in the Biologic SFM/4000/S stopped flow reactor was 1.5 mm and dead time of the system was 1.4 ms. The system was cooled and maintained at 4□C. Reaction mixtures contained 400 µM of mb-SB2 and either 40, 100, 200, 240, 280, 320, 360, 400, 600, 700, or 800 µM of HAuCl4. For displacement reactions contained 400 M Cu-mb-SB2 and 400 µM HAuCl4. Rates obtained for each concentration were an average of either 5 or 7 traces. The rates were determined by fitting the traces to the exponential function in Biokine operational software (Bio-Logic Science Instrument SA). Binding rates were calculated in mol Au bound per sec per mol mb-SB2 and reported as the binding number (s^{-1}). The binding rates for mb-OB3b were calculated in the same way resulting in mol Au^{3+} bound per sec per mol mb-OB3b, also reported as a binding number with units of s-1.

Metal displacement

Equimolar concentrations of HAuCl4 or $CuCl_2$ were added to mb- SB followed by the addition of equimolar concentrations of, either CuSO4 or HAuCl4, respectively. The UV-visible absorption spectra were determined immediately after mixing. The potential displacement of Au^{3+} by Cu^{2+} or Cu^{2+} by Au^{3+} was also determined by metal analysis as described by Baral et al [17].

Cu^{2+} and Au^{2+} binding in mixed-metal solutions

Binding of Au^{3+} and Cu^{2+} in mixed metal solution by mb-SB2 was determined in solutions containing CuSO4, HAuCl4 and mb-SB2 in molar ratios of 0.25:0.25:1, 0.5:0.5:1, 1:1:1, 1.5:1.5:1, and 2:2:1, respectively. Solutions were incubated with stirring (200 rpm) at room temperature for 5 min. Following this incubation period, the samples were loaded to pre-equilibrated Sep-Pak cartridges as previously described [5]. Sep-Pak cartridges were washed with 6 ml of >18MΩ▪cm H2O three times then eluted with 6 ml of 60% acetonitrile : 40% H2O. Copper and gold concentrations were determined by atomic absorption spectroscopy as described by Baral et al [17]. In addition to the sample eluting in 60% acetonitrile : 40% H2O, gold and copper concentrations were determined directly from the reaction mixture as well as H2O wash solution. Similarly, copper and gold measurements were performed on control solutions containing: i) gold and copper only, ii) gold and mb-SB2 only and iii) copper and mb-SB2 only.

Acknowledgements

We thank V. Frasca at GE Microcal for assistance in modeling the ITC results. This research was supported by the Office of Science (BER), U.S. Department of Energy (JDS and ADS and the National Science Foundation (CHE10112271) (ADS) . Use of the ITC and stopped-flow spectrophotometer were made possible through a generous gift from the Roy J. Carver Charitable Trust (Muscatine, Iowa).

References

[1] Kim, H. J.; Graham, D. W.; DiSpirito, A. A.; Alterman, M. A.; Galeva, N.; Larive, C. K.; Asunskis, D.; Sherwood, P. M. *Science* **2004**, *305*, 1612.

[2] Krentz, B. D.; Mulheron, H. J.; Semrau, J. D.; DiSpirito, A. A.; Bandow, N. L.; Haft, D. H.; Vuilleumier, S.; Murrell, J. C.; McEllistrem, M. T.; Hartsel, S. C.; Gallagher, W. H. *Biochemistry* **2010**, *49*, 10117.

[3] El Ghazouani, A.; Basle, A.; Firbank, S. J.; Knapp, C. W.; Gray, J.; Graham, D. W.; Dennison, C. *Inorg. Chem.* **2011**, *50*, 1378.

[4] El Ghazouani, A.; Basle, A.; Gray, J.; Graham, D. W.; Firbank, S. J.; Dennison, C. *P Natl Acad Sci USA* **2012**, *109*, 8400.

[5] DiSpirito, A. A.; Semaru, J. D.; Murrell, J. C.; Gallagher, W. H.; Dennison, C.; Vuilleumier, S. *Microbiol. Mol. Biol. Rev.* **2016**, *80*, 387.

[6] Choi, D. W.; Zea, C. J.; Do, Y. S.; Semrau, J. D.; Antholine, W. E.; Hargrove, M. S.; Pohl, N. L.; Boyd, E. S.; Geesey, G. G.; Hartsel, S. C.; Shafe, P. H.; McEllistrem, M. T.; Kisting, C. J.; Campbell, D.; Rao, V.; de la Mora, A. M.; Dispirito, A. A. *Biochemistry* **2006**, *45*, 1442.

[7] Choi, D. W.; Do, Y. S.; Zea, C. J.; McEllistrem, M. T.; Lee, S. W.; Semrau, J. D.; Pohl, N. L.; Kisting, C. J.; Scardino, L. L.; Hartsel, S. C.; Boyd, E. S.; Geesey, G. G.; Riedel, T. P.; Shafe, P. H.; Kranski, K. A.; Tritsch, J. R.; Antholine, W. E.; DiSpirito, A. A. *J Inorg Biochem* **2006**, *100*, 2150.

[8] Baral, B. S.; Bandow, N. L.; Vorobev, A.; Freemeier, B. C.; Bergman, B. H.; Herdendorf, T.; Fuentes, N.; Ellias, L.; Turpin, E.; Semrau, J. D.; Di Spirito, A. A. *J. Inorgan. Biochem.* **2014**, *141*, 161

[9] Bandow, Nathan, "Isolation and binding properties of methanobactin from the facultative methanotroph Methylocystis strain SB2" (2014). Graduate Theses and Dissertations. Paper 13910.

[10] Vorobev, A.; Jagadevan, S.; Baral, B. S.; Dispirito, A. A.; Freemeier, B. C.; Bergman, B. H.; Bandow, N. L.; Semrau, J. D. *Appl Environ Microb* **2013**, *79*, 5918.

[11] Lightner, D. A.; Gurst, J. E. *Organic Conformational Analysis and Steriochemistry from Circular Dichroism Spectroscopy*; Wiley-VCH: New York, NY, USA, 2000.

[12] Kim, H. J.; Galeva, N.; Larive, C. K.; Alterman, M.; Graham, D. W. *Biochemistry* **2005**, *44*, 5140.

[13] Bandow, N.; Gilles, V. S.; Freesmeier, B.; Semrau, J. D.; Krentz, B.; Gallaghe, W.; McEllistrem, M. T.; Hartse, S. C.; Cho, D. W.; Hargrove, M. S.; Heard, T. M.; Chesner, L. M.; Braunreiter, K. M.; Cao, B. V.; Gavitt , M. M.; Hoopes, J. Z.; Johnson, J. M.; Polster, E. M.; Schoenick, B. D.; A.M., U.; DiSpirito, A. A. *J. Inorgan. Biochem.* **2012**, *110*, 72

[14] Berova, N.; Di Bari, L.; Pescitelli, G. *Chem. Soc. Rev.* **2007**, *36*, 914

[15] Elango, N.; Radhakrishnan, R.; Froland, W. A.; Wallar, B. J.; Earhart, C. A.; Lipscomb, J. D.; Ohlendorf, D. H. *Protein Sc.* **1997**, *6*, 556

[16] Bandow, N.; Gilles, V. S.; Freesmeier, B.; Semrau, J. D.; Krentz, B.; Gallagher, W.; McEllistrem, M. T.; Hartsel, S. C.; Choi, D. W.; Hargrove, M. S.; Heard, T. M.; Chesner, L. N.; Braunreiter, K. M.; Cao, B. V.; Gavitt, M. M.; Hoopes, J. Z.; Johnson, J. M.; Polster, E. M.; Schoenick, B. D.; Umlauf, A. M.; DiSpirito, A. A. *J. Inorg. Biochem.* **2012**, *110*, 72–82.

[17] Baral, B. S.; Bandow, N.; Vorobev, A.; Freesmeier, B. C.; Bergman, B. H.; Herdendorf, T. J.; Fuentes, N.; Ellias, L.; Turpin, E.; Semrau, J. D.; DiSpirito, A. A.*J. Inorg. Biochem.* **2014**, *141C*, 161–169.

[18] Bielski, B.H., Cabelli, D.E., Arundi, R.L., Ross, A.A. *J. Phys. Chem. Ref. Data.* **1985**, *14*, 1041 - 1100.

[19] Shelley, E. J.; Ryan, D.; Johnson, S. R.; Couillard, M.; Fitzmaurice, D.; Nellist, P. D.; Chen, Y.; Palmer, R. E.; Preece, J. A. *Langmuir* **2002**, *18*, 1791–1795.

[20] Frens, G. *Nat Phys Sci* **1973**, *241*, 20–22.

Figures

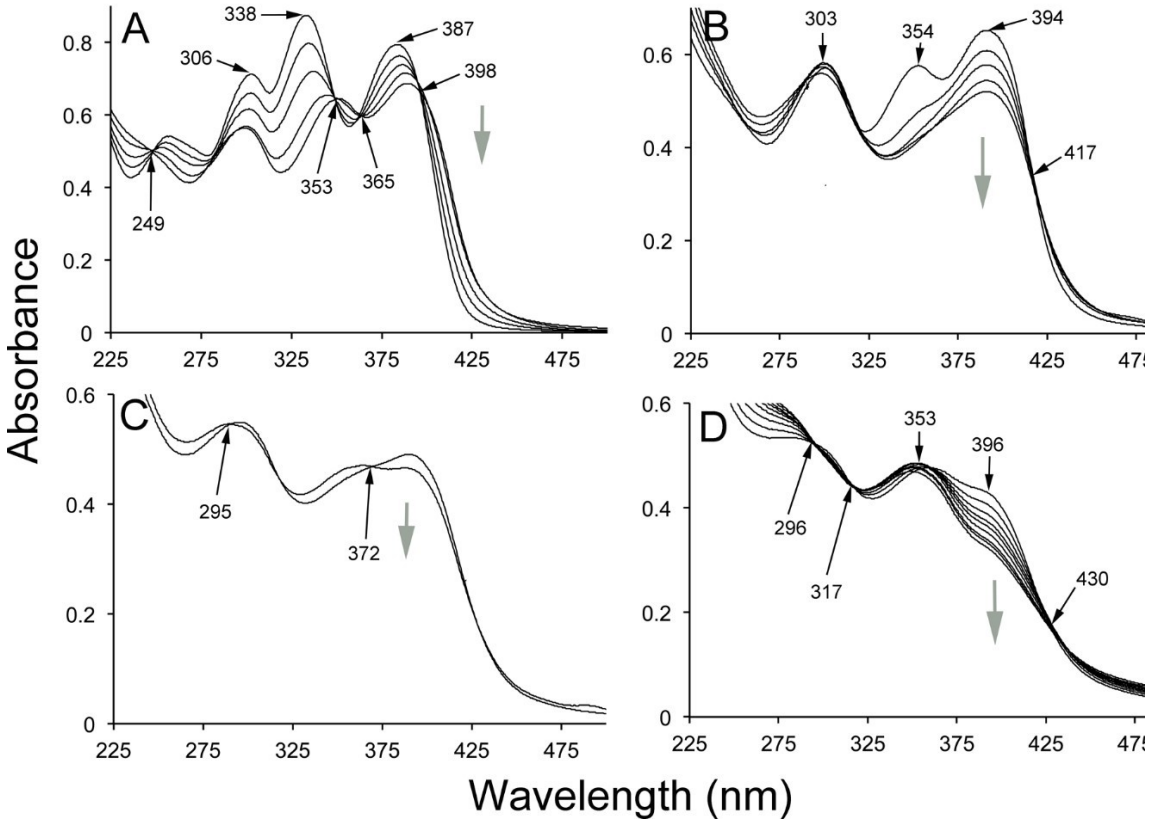

Figure 1. UV-visible absorption spectra of mb-SB2 as isolated and following the addition of 0.1, 0.2, 0.3, and 0.4 molar additions of HAuCl4 (**A**); 0.5, 0.6, 0.7 and 0.8 molar additions of HAuCl4 (**B**); 1.0 and 1.1 molar additions of HAuCl4 (**C**); and 1.2 to 2.3 molar additions of HAuCl4 (**D**).

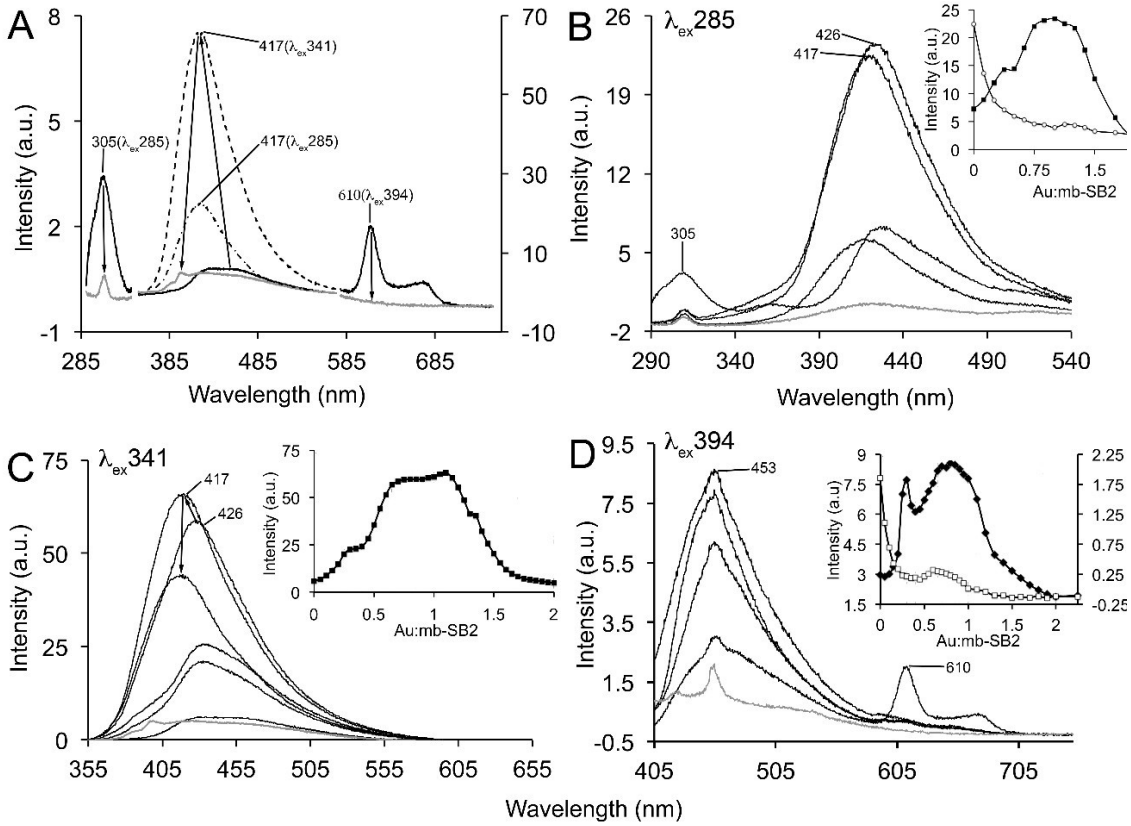

Figure 2. Emission spectra from SB2-mb **(A)** following excitation at 285 **(B)** 341 **(C)** and 394 nm **(D)** as isolated and following $HAuCl_4$ additions. Inserts: **(B)** emission intensities at 305 (○) and 417/426 (■) following excitation at 285 nm; **(C)** emission intensities at 417/426 (■) nm following excitation at 341 nm; and **(D)** emission intensities at 453 (◇) and 610 (■) nm following excitation 394 nm.

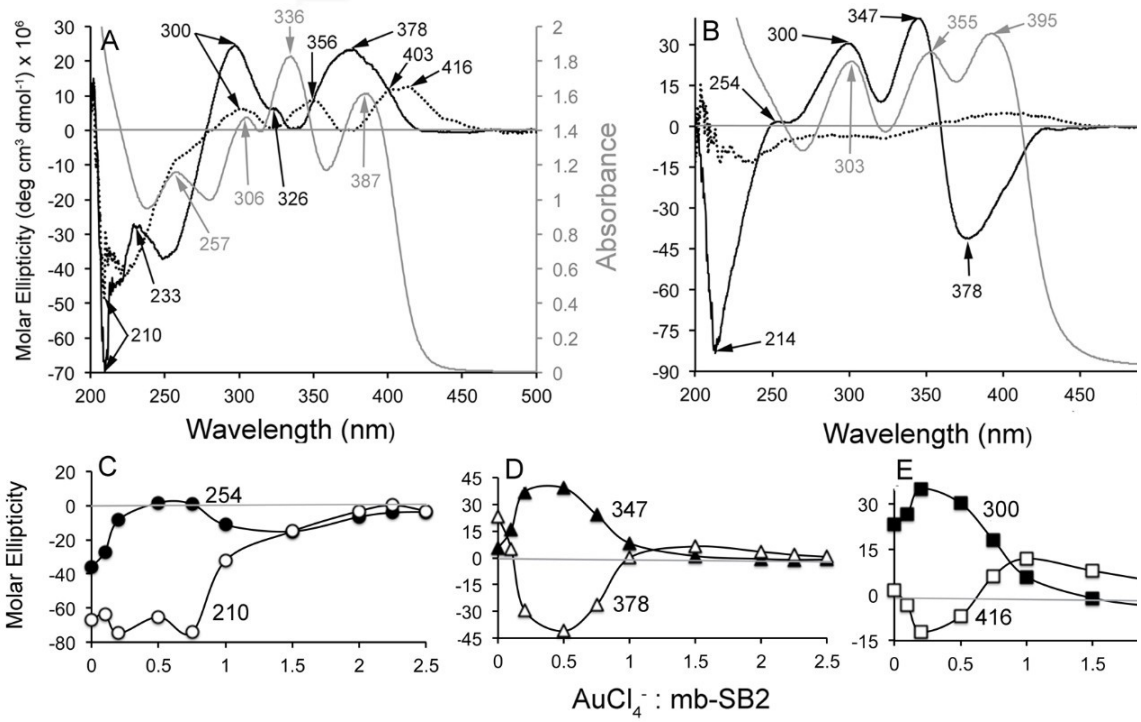

Figure 3. UV-visible absorption (——) and UV-visible CD spectra (———) of mb-SB2 (**A**) as isolated, no $AuCl_4^-$ added; and (**B**) following the addition of equimolar $AuCl_4^-$. Changes in molar ellipticity at (**C**) 210 and 254 nm; (**D**) 347 and 378 nm; (**E**) 300 and 416 nm.

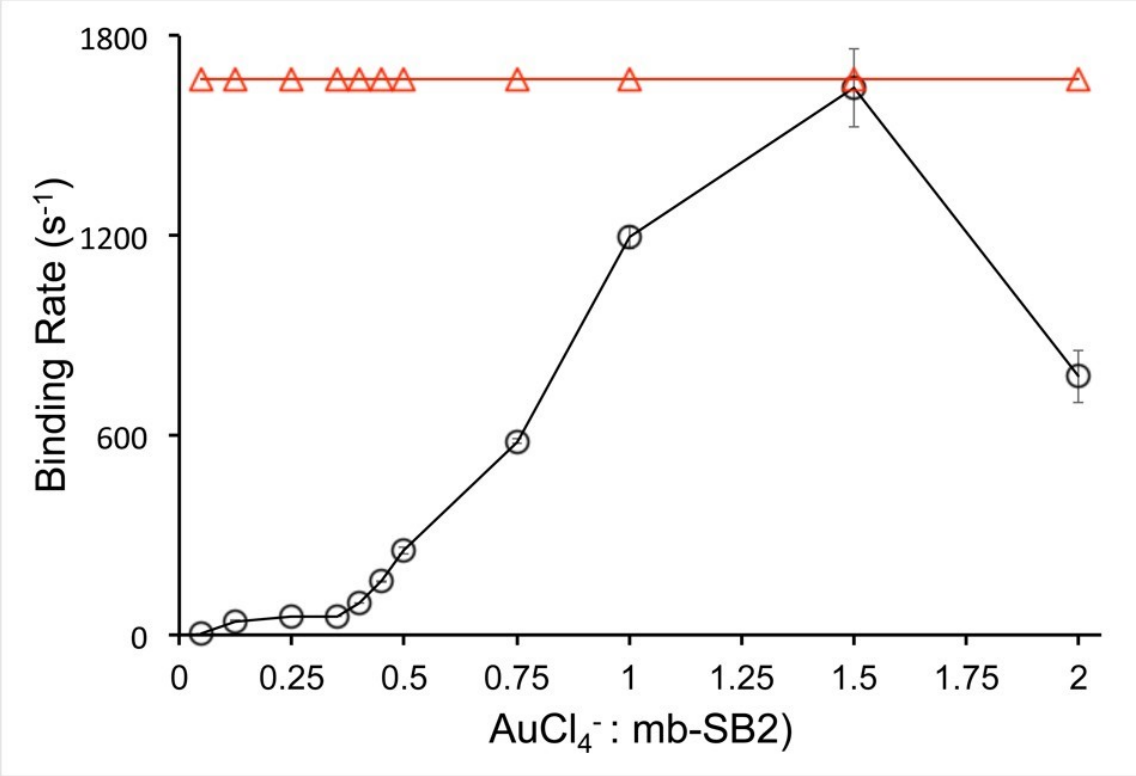

Figure 4. Rate of $AuCl_4^-$ coordination by mb-SB2 at 4°C for the imidazolone and oxazolone rings, corresponding to the stopped flow traces collected at 389 (△) and 341 (○) nm, respectively.

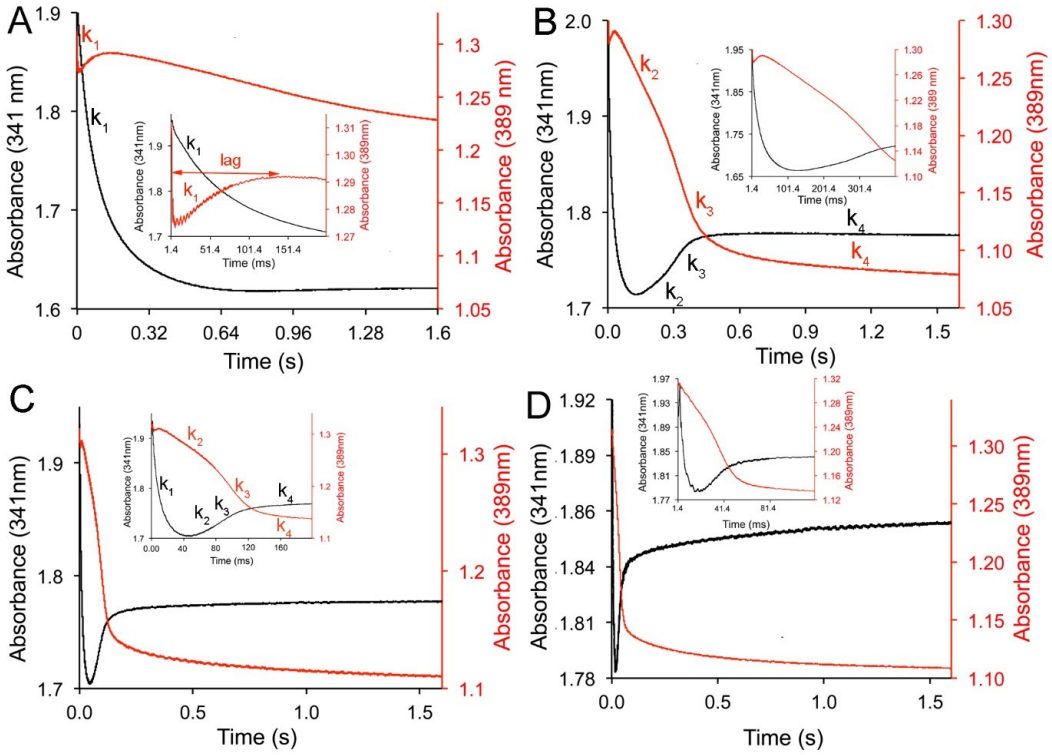

Figure 5. Stopped-flow traces for $AuCl_4^-$ binding by mb-OB3b, collected using a four-syringe Biologic SFM/4000/S stopped flow reactor coupled to a MOS-500 spectrophotometer (Bio-Logic Science Instrument SA, Claix, France), at 341 nm (Oxazalone B, Black) and 389 nm (Oxazalone A, Red) for mole ratios, (**A**) 0.25, (**B**) 0.50, **C**) 1.0, and **D**) 2.0; system was cooled to 4° C.

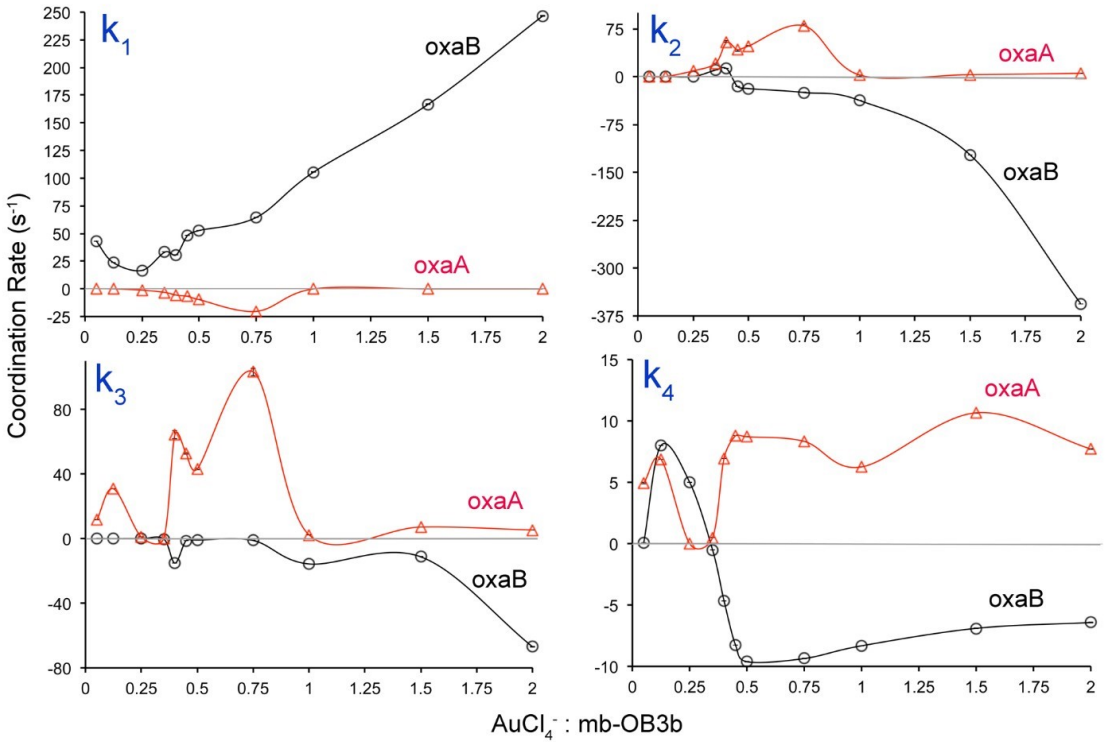

Figure 6. Rate of $AuCl_4^-$ coordination by mb-OB3b at 4°C, for the coordination events: **(A)** k1; (**B**) k2; (**C**) k3; and (**D**) k4, by oxazolone A and oxazolone B, corresponding to the stopped flow traces collected at 389 and 341 nm, respectively.

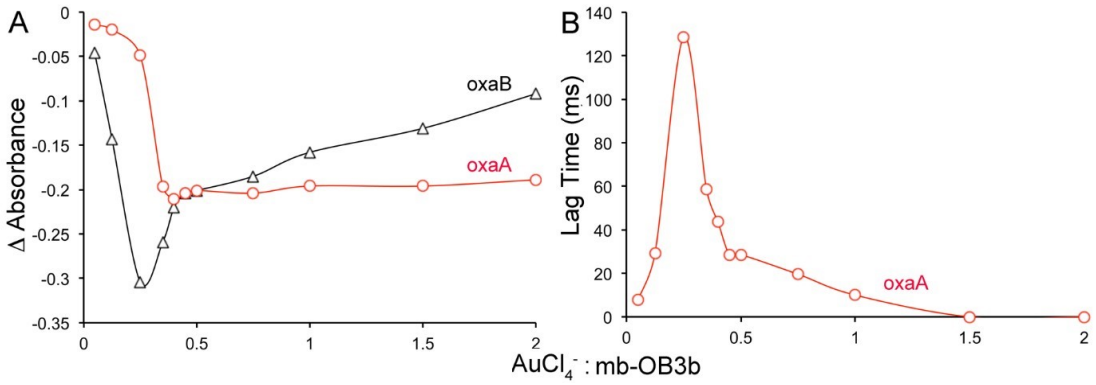

Figure 7. (**A**) Change in absorbance calculated for the initial binding event and (**B**) the calculated lag time before $AuCl_4^-$ binding by the oxazolone A ring of mb-OB3b.

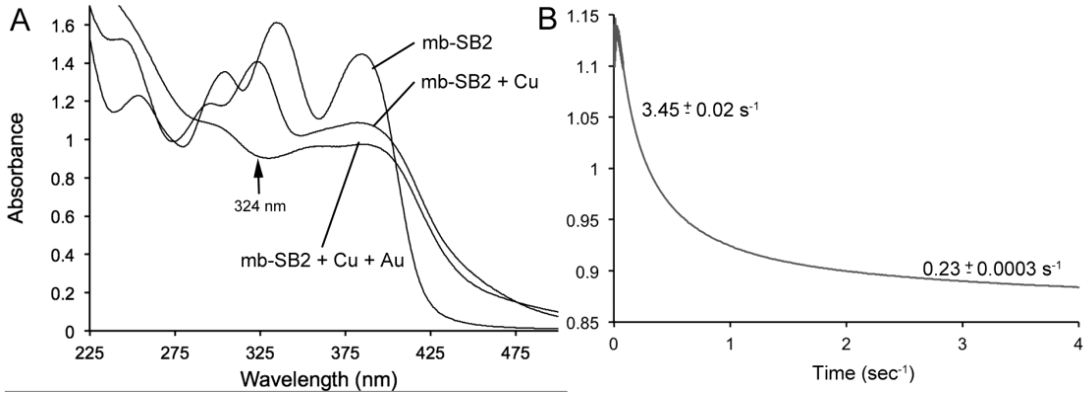

Figure 8. (**A**) UV-visible absorption spectrum of mb-SB2 as isolated following the addition of equimolar concentrations of Cu^{2+}, and following the addition of equimolar oncentrations of Au^{3+} to Cu-mb-SB2. (**B**) Absorbance changes at 324 nm following the addition of equimolar concentrations of Au^{3+} to Cu-mb-SB2 at 4˚C.

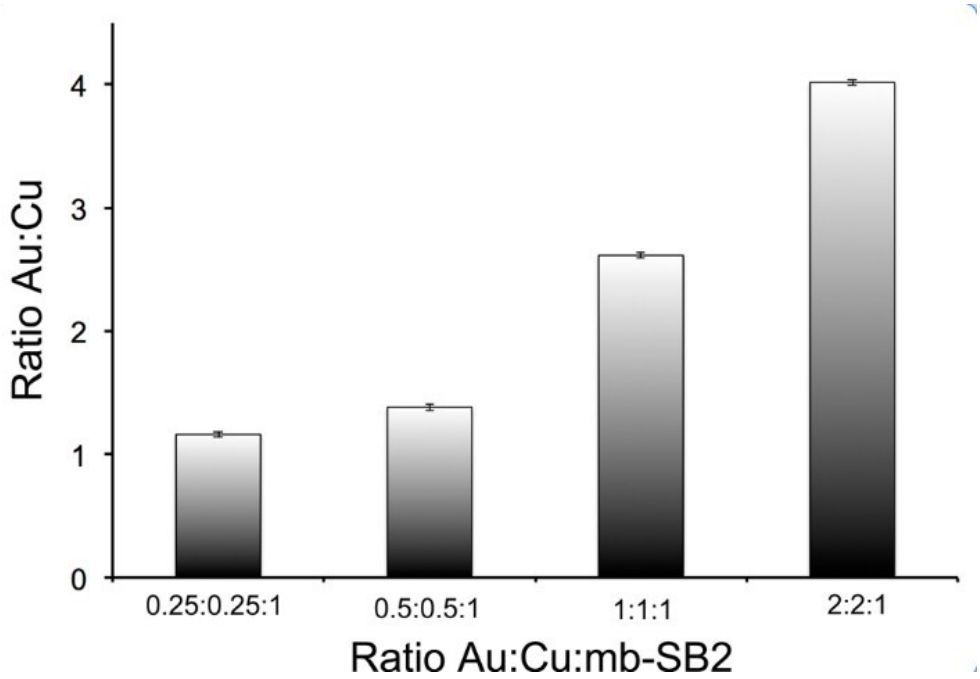

Figure 9. Ratio of Au to Cu bound to mb-SB2 following incubation of mb-SB2 in solutions containing Cu^{2+}, Au^{3+} and mb-SB2 in molar ratios of 0.25:0.25:1, 0.5:0.5:1, 1:1:1, 1.5:1.5:1, and 2:2:1, respectively. Error bars represent the pooled standard deviations.

Supplemental Material

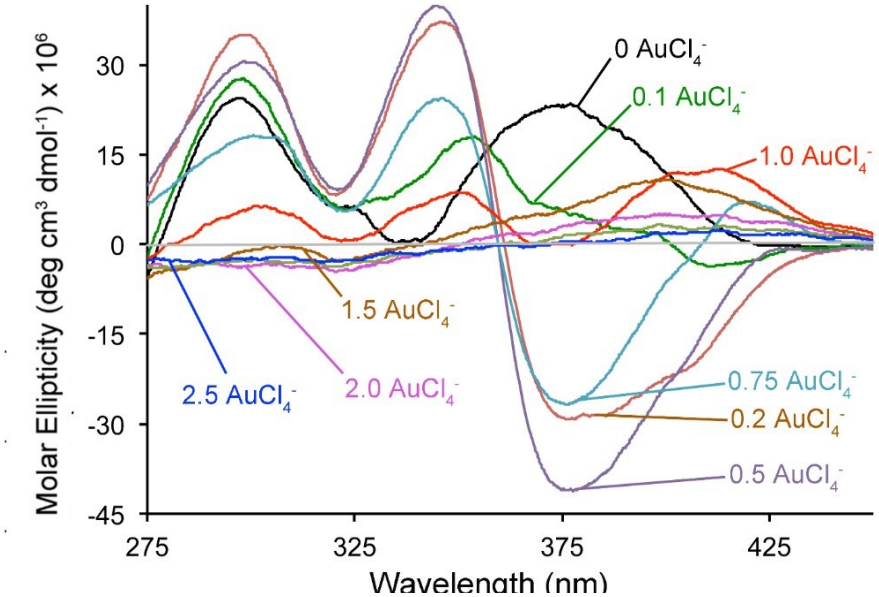

Figure S1. Circular dichroism (CD) titration spectra for $AuCl_4^-$ binding by mb-SB2 for all mole ratios, $AuCl_4^-$: mb-SB2, collected for this titration; range 0 – 2.5.